Controlling Coupled Chemical Oscillators: Toward Synchronization Engineering and Chemical Computation

Senior Thesis

Presented to

The Faculty of the School of Arts and Sciences

Brandeis University

Undergraduate Program in Physics

In Partial Fulfillment of the Requirements for the Degree of Bachelor of Science

by

Adam L. Wang

Advisor:

Seth Fraden

May, 2015

To my family

Abstract

The collective behaviors of coupled oscillators are ubiquitous in biological systems, with examples including quorum sensing, cardiac muscle contractions, and networks of neurons. In an effort to better understand the generic properties of such oscillators, we investigated emulsions of diffusively coupled microdroplets containing the oscillatory Belousov—Zhabotinsky (BZ) reaction with a photo-inhibitive catalyst. We created packed 2D arrays of BZ droplets via microfluidic techniques and studied the behavior of particular geometries with optically-induced boundary conditions. We used optical perturbations to alter periods and phases of oscillation in a controlled fashion, and also to completely suppress oscillations in the BZ droplets. Furthermore, we exploited the observed inhibitory coupling to establish a basis for computation through a chemical substrate by creating a functional NOR gate in a simple 1D arrangement of three BZ droplets.

Contents

List of Figures

List of Tables

Chapter 1

Introduction

Synchronization is a universal phenomena that is characterized by order in time. It occurs at all scales of the universe, ranging from electrons moving simultaneously in superconductors to massive asteroids hurled by gravitational synchrony [1]. Even more interesting is spontaneous synchronization that dates back to 1665 when Christiaan Huygens observed that two pendulums mounted on the same support synchronized and moreover, if disturbed, re-synchronized [2]. It is quite a mysterious phenomena, especially since according to thermodynamics nature prefers states of higher entropy, yet ordered synchronization can be seen in many biological systems including networks of fireflies that flash in a synchronous fashion [3], pacemaker cells that control heart rate [4], quorum sensing that allows bacteria and other social organisms to communicate [5, 6, 7], networks of neurons [8], and even spontaneous synchronization of human interactions such as walking, bodily gestures, and facial expression [9, 10, 11].

Many of the above examples can be described by a mathematical framework that studies the interactions between coupled oscillators, which has become one of the most important topics of study in nonlinear dynamics. Several textbooks have been written with more examples and analysis of such systems [12, 13, 14, 15, 16]. For two coupled oscillators, the math is quite tractable, but the systems mentioned previously consist of hundreds, even

thousands of coupled oscillators where no analytic solution exists and much of their behavior cannot even be described qualitatively. Despite their prevalence, there is a relatively small number of experimental systems to study networks of coupled oscillators; ours is one such system.

We use a reaction—diffusion system consisting of a monodisperse emulsion of micro-droplets (50 to 200 μm in diameter) containing the oscillatory Belousov—Zhabotinsky (BZ) reaction. Their small size allows us to assume they are uniform in concentration and hence we can ignore spatial oscillations. The droplets are separated by a surfactant-stabilized oil that allows for diffusion of non-polar species allowing chemo-selective coupling. In particular, Br_2 most strongly partitions through the oil into neighboring droplets and results in inhibitory coupling between these chemical oscillators. Oscillators coupled via inhibition will be the focus in this thesis, though our system can be readily adapted to include excitatory coupling by changing properties of the oil [17] and microfluidic methods by using, for example, PDMS which Br_2 can diffuse through. We also add a photo-catalyst, $Ru(bipy)_3$, that allows blue light to inhibit the oscillations. Using a programmable illumination microscope (PIM), we are able to engineer geometries with optically induced constant-chemical concentration boundary conditions, set initial conditions, and perturb oscillators in a controlled fashion.

A second route we are taking is geared toward computation, specifically chemical computation. We have demonstrated a chemical NOR gate composed of three BZ micro-droplets; this is significant because a NOR gate is functionally complete in the sense that any computational operation can be implemented using only NOR gates [18]. In addition, we are working toward programmable, self-driven chemomechanical action to mimic biological processes like the beating of a heart and to serve as a model system for the growing field of soft, active matter. There is much interest toward construction of robots for performing a wide range of activities from surgery [19] to unmanned transportation [20]. Traditional hard robots, however, have difficulty handling fragile objects and moving across unmapped, dynamic terrain which would be encountered, for example, near vital internal organs. Soft robots have been

proposed as a solution to these problems [21, 22, 23, 24] and typically undergo a volume change [25, 26]. Gels based on the BZ reaction have been synthesized that exhibit tunable volume oscillations, dependent on temperature and chemistry [27, 28]. We hope to integrate a BZ emulsion within a gel whose dynamics will govern the gel's oscillations. The emulsion acts as a brain that, used in conjunction with optical perturbations, may generate directed volume changes for locomotion.

In Chapter 2, we will give background information and discuss the mechanism underlying the BZ reaction. We will also present a simplified chemical model and describe the mathematical framework we use for simulations. Finally, we will introduce the notion of phase and how it is a useful descriptor for any oscillator.

In Chapter 3, we will present the reactants we use in our version of the BZ reaction and methods to create our emulsions. We will then discuss the PIM and its critical role in data analysis and optical perturbations.

In Chapter 4, we will discuss the behaviors of oscillators coupled via inhibition as observed in experiment. We will then present results demonstrating our abilities to engineer particular geometries and optically perturb oscillators with light, as well as planned future work for synchronization engineering.

In Chapter 5, we will define our chemical NOR gate and demonstrate its functionality in experiment. We will also propose ways to improve upon its robustness and connect multiple gates together.

Chapter 2

The Belousov–Zhabotinsky Reaction

The Belousov–Zhabotinsky (BZ) reaction is an oscillating chemical reaction first discovered by Boris Pavlovich Belousov in the 1950s [29]. It consists of a metal ion-catalyzed oscillatory oxidation of an organic substrate, typically malonic acid, by bromate in an acidic medium. It is an example of a chemical system that can operate far from equilibrium for a significant amount of time and has consequently impacted the field of non-equilibrium thermodynamics; today it is used as a prototypical system to study nonlinear dynamics [30, 31].

Initially, Belousov's discovery was so surprising that he was not accredited until several years after his death on the grounds that such a system "was quite impossible"[32]. Since chemical reactions generally proceed in one direction, it is unusual to witness a reaction that continually reverses and seems to oscillate about an equilibrium point. This would violate the second law of thermodynamics since entropy is a maximum at equilibrium and hence once reached, a system cannot spontaneously deviate from there. However, this does not rule out the possibility that a system can oscillate toward equilibrium. Indeed it is now well understood that chemical oscillators do exist, but only if they are far from equilibrium [12]. The oscillations are accompanied by an overall increase in entropy generated by energy releasing reactions that typically follow two pathways: one involving an auto-catalytic process and a second that inhibits the autocatalysis. Furthermore, intermediates produced can

signal a switch between the two pathways.

A sequence of images displaying a continuously stirred beaker of BZ is shown in Figure 2.1. The blue color change is due to the auto-catalytic oxidation of catalyst, corresponding to the oxidized state, while the red color corresponds to the reduced state, where the oxidized catalyst is being reduced. It is interesting to note that the BZ reaction can also exhibit spatial oscillations using a layer of unstirred BZ in, for instance, a petri dish [12]. Concentric and spiral waves form that then collide and annihilate. Even Turing patterns, patterns that are periodic in space but stationary in time, have been observed [33]. In this thesis, however, we will focus on homogeneous reactors such that only temporal oscillations are observed. The rest of this chapter will discuss the key features exhibited by our BZ system and computational methods to model its behavior.

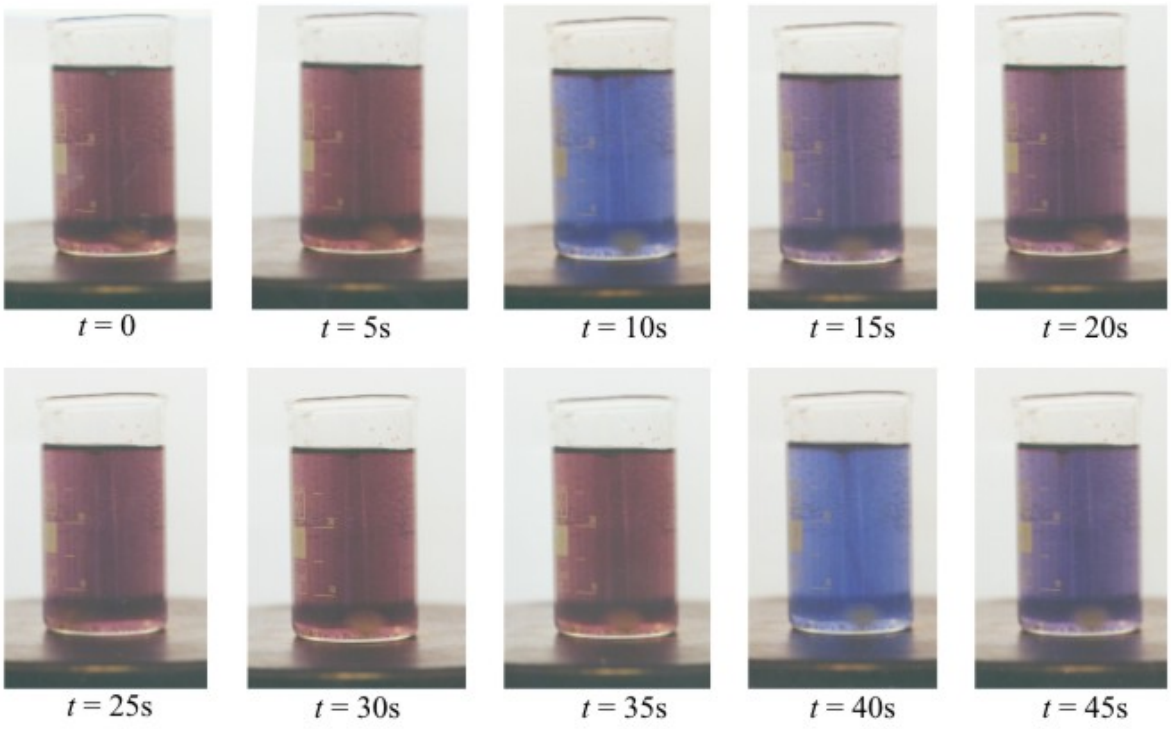

Figure 2.1: Sequence of images of a continuously stirred beaker of ferroin-catalyzed BZ demonstrating periodic oscillations, signified by a blue color change. The blue color indicates the reaction is in the oxidized state while the red color indicates it is in the reduced state.

Table 2.1: List of BZ reactants used in our system.

Name	Chemical Formula
Malonic Acid	$CH_2(COOH)_2$
Sulfuric Acid	H_2SO_4
Sodium Bromide	$NaBr$
Sodium Bromate	$NaBrO_3$
Ferroin	$C_{36}H_{24}FeN_6^{2+}$
$Ru(bipy)_3$	$C_{30}H_{24}N_6Cl_2Ru{\cdot}6H_2O$

2.1 Chemical Mechanism

Our version of the BZ reaction consists of six reactants listed in Table 2.1 where ferroin and $Ru(bipy)_3$ are short-hand for ferroin redox indicator (1, 10 - phenanthroline iron(II) sulfate complex) and tris(bipyridine)ruthenium(II) chloride, respectively. The BZ mechanism responsible for temporal oscillations in its entirety is extremely complicated, with models containing as many as 80 elementary reactions and 26 chemical concentration variables [34]. One popular simplification to 7 variables, first proposed by Richard Field, Endre Körös, and Richard Noyes of the University of Oregon, is aptly known as the FKN mechanism [35]. The analysis is based on a cerium-catalyzed system, but Zhabotinsky showed that various ion complexes can be used as well, including ferroin [36].

A key feature of the BZ reaction is the auto-catalytic oxidation of a catalyst (ferroin) combined with inhibition of the oxidation via a chemical intermediate (Br^-). A qualitative description containing the essential mechanism consists of the following three processes:

Process 1. Consumption of inhibitor (Br^-).

Process 2. Auto-catalytic oxidation of ferroin.

Process 3. Simultaneous reduction of ferriin and production of inhibitor (Br^-).

Once all the ferriin is reduced, there is no longer production of inhibitor. As a result, there is a net consumption of inhibitor which signifies the return to Process 1 and the cycle repeats.

Equations (2.1) through (2.5) demonstrate a few representative reactions for each process.

Process 1.

$$2H^+ + BrO_3^- + Br^- \rightarrow HBrO_2 + HOBr \tag{2.1}$$

$$H^+ + HBrO_2 + Br^- \rightarrow 2HOBr \tag{2.2}$$

Process 2.

$$H^+ + BrO_2^\bullet + Fe(phen)_3^{2+} \rightarrow Fe(phen)_3^{3+} + HBrO_2 \tag{2.3}$$

Process 3.

$$2H_2O + BrCH_2(COOH)_2 + 4Fe(phen)_3^{3+} \rightarrow 4Fe(phen)_3^{2+} + Br^- + HCOOH + 2CO_2 + 5H^+ \tag{2.4}$$

$$2H_2O + CH_2(COOH)_2 + 6Fe(phen)_3^{3+} \rightarrow 6Fe(phen)_3^{2+} + HCOOH + 2CO_2 + 6H^+ \tag{2.5}$$

Another major set of reaction we must consider involve $Ru(bipy)_3$, a photo-sensitive catalyst. It has been shown that light at the wavelength $\lambda = 452$ nm excites the ruthenium catalyst and causes a series of photo-chemical reactions in the BZ system that produce bromide, the inhibitor [37, 38, 39]. The reactions are as follows:

$$Ru(bipy)_3^{2+} + h\nu \rightarrow Ru(bipy)_3^{2+*} \tag{2.6}$$

$$BrCH_2(COOH)_2 + Ru(bipy)_3^{2+*} \rightarrow Ru(bipy)_3^{3+} + Br^- \tag{2.7}$$

$$Ru(bipy)_3^{2+*} \rightarrow Ru(bipy)_3^{2+} \tag{2.8}$$

Using $Ru(bipy)_3$, it is possible to extend the period of oscillation and even suppress the auto-catalytic oxidation entirely via optical perturbations. This photo-inhibition will prove to be useful in synchronization engineering and chemical computation, as will be discussed in Chapter 4 and Chapter 5.

2.2 Chemical Model

Using the FKN mechanism described in Section 2.1 and ignoring spatial oscillations, a set of seven ordinary differential equations can be constructed that models the reaction with a relatively high degree of accuracy [39]. The drawback is that for large simulations containing multiple interacting oscillators, the FKN model requires long execution times. Further simplification to three variables has been made, constituting the Oregonator model of BZ [40]. However, certain phenomena are not captured [39]. To remedy this but still maintain a computationally efficient model, Vladimir Vanag and Irving Epstein developed a four-variable model of BZ. The four concentration variables are $x = [\mathrm{HBrO_2}], y = [\mathrm{Br^-}], z = [\text{oxidized catalyst}]$, and $u = [\mathrm{Br_2}]$. The Vanag-Epstein (VE) model is as follows:

$$\frac{dx}{dt} = -k_1 xy + k_2 y - 2k_3 x^2 + k_4 \frac{x(c_0 - z)}{c_0 - z + c_{\min}} \tag{2.9}$$

$$\frac{dy}{dt} = -3k_1 xy - 2k_2 y - k_3 x^2 + k_7 u + k_9 z + k(I) \frac{c_0 - z}{b_C/b + 1} \tag{2.10}$$

$$\frac{dz}{dt} = 2k_4 \frac{x(c_0 - z)}{c_0 - z + c_{\min}} - k_9 z - k_{10} z + k(I) \frac{c_0 - z}{b_C/b + 1} \tag{2.11}$$

$$\frac{du}{dt} = 2k_1 xy + k_2 y + k_3 x^2 - k_7 u \tag{2.12}$$

Rate constants are denoted by k with a subscript, c_0 is the total concentration of catalyst,[1] $c_{\min} = \sqrt{2k_r(k_9 + k_{10})c_0}/k_{\mathrm{red}}$ and $b = [\mathrm{BrCH_2(COOH)_2}]$, all of which are taken to be constants. Also, $k(I)$ is the rate of excitation of $\mathrm{Ru(bipy)_3^{2+}}$ as given in Equation (2.6) and is a function of the light intensity. More details can be found in the original paper [39].

As an example, Figure 2.2 displays the steady-state chemical concentrations as simulated by the VE model. Notice the auto-catalytic oxidation of catalyst (z) that is quickly suppressed by the presence of bromide ion (y). The oxidation then resumes once all bromide has decayed away.

[1]The model assumes only one photo-sensitive catalyst, though in experiment there are two: ferroin and $\mathrm{Ru(bipy)_3}$. We use ferroin in addition to $\mathrm{Ru(bipy)_3}$ because it produces a sharp color change that allows us to measure precisely when oxidation spikes occur, as will be discussed in Chapter 3, Section 3.3.

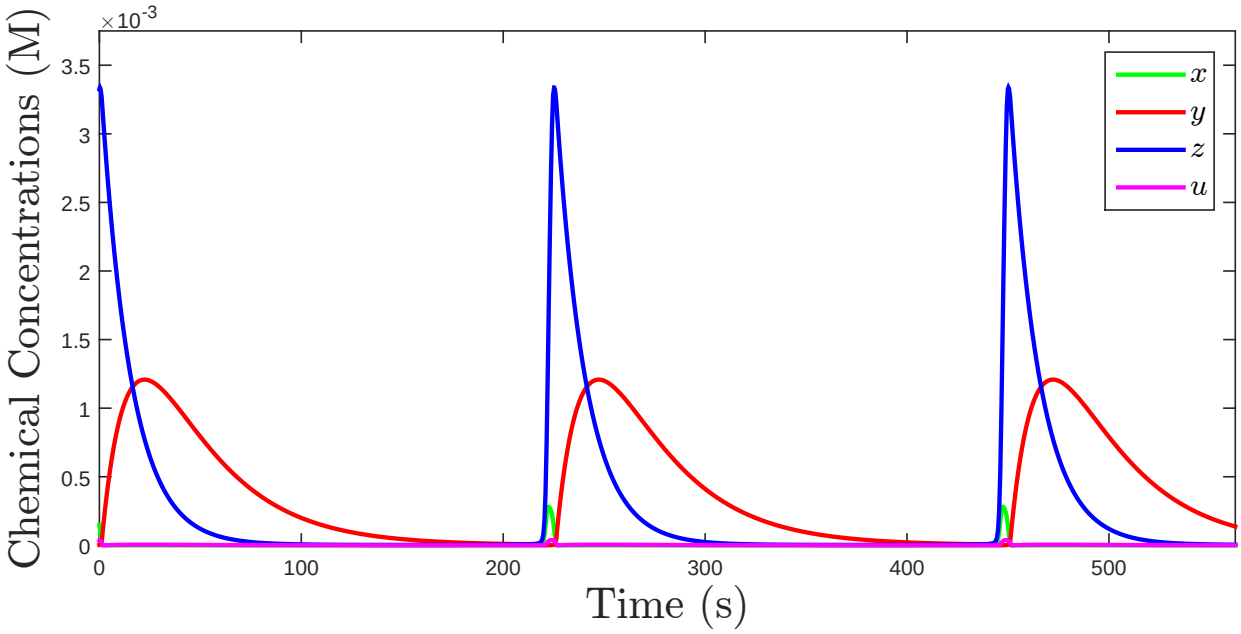

Figure 2.2: Simulated chemical concentrations using the VE model where: $x = [\mathrm{HBrO_2}]$, $y = [\mathrm{Br^-}]$, $z =$ [oxidized catalyst], and $u = [\mathrm{Br_2}]$.

2.3 Modeling Coupled Oscillators

If we assume an oscillator to be a point with uniform chemical concentration, then the kinetics governing a single oscillator can be written compactly as

$$\frac{d\boldsymbol{c}}{dt} = \boldsymbol{R}(\boldsymbol{c}) \tag{2.13}$$

where $\boldsymbol{c}$ is a vector containing all n chemical species and $\boldsymbol{R} : \mathbb{R}^n \mapsto \mathbb{R}^n$ is a vector function that describes the reaction kinetics governing each species c_k, namely

$$\boldsymbol{R}(\boldsymbol{c}) = \sum_{k=1}^{n} \frac{dc_k}{dt} \hat{\boldsymbol{e}}_k. \tag{2.14}$$

Explicitly in the VE model,

$$\boldsymbol{c} = [x, y, z, u] \quad \text{and} \quad \boldsymbol{R}(\boldsymbol{c}) = [\dot{x}, \dot{y}, \dot{z}, \dot{u}], \tag{2.15}$$

where $\dot{x}, \dot{y}, \dot{z}$, and $\dot{u}$ are defined by Equations (2.9) through (2.12).

When considering coupled oscillators, we must account for the effects of diffusion between them. In one-dimension, Fick's law states that

$$J = -D\frac{\partial \phi}{\partial x} \tag{2.16}$$

where J is the diffusion flux, D is the diffusion coefficient, ϕ is the concentration, and x is the spatial coordinate. Thus, the flow is directed from regions of high concentration to regions of low concentration and its magnitude is proportional to the gradient. We also make the following two assumptions in our model:

Assumption 1. Each oscillator is small enough such that it is chemically homogeneous.

Assumption 2. Chemicals do not accumulate in the medium between oscillators.

The kinetics for N coupled oscillators are then given by a system of equations of the form

$$\frac{d\boldsymbol{c}_i}{dt} = \boldsymbol{R}(\boldsymbol{c}_i) + \boldsymbol{D}\sum_{j=1}^{N} A_{ij}\left(\boldsymbol{c}_j - \boldsymbol{c}_i\right) \tag{2.17}$$

where $\boldsymbol{c}_i$ is a vector containing all chemical species in the i-th oscillator, A_{ij} is an element in the $N \times N$ adjacency matrix $\boldsymbol{A}$ that depends on the network and is equal to one if droplet i and j are coupled and zero if they are uncoupled, and $\boldsymbol{D}$ is a $n \times n$ diagonal matrix containing the coefficients of diffusive transport for each chemical species. The coefficient of diffusive transport (μ) is proportional to the diffusion coefficient and depends on the geometry of the system as well as the diffusion and partition coefficients of each chemical species. Equation (2.17) tells us that the time evolution of each oscillator is governed by a reaction within, $\boldsymbol{R}(\boldsymbol{c}_i)$, and diffusion from neighbors, hence describing a reaction-diffusion system. Notice in the special case where $N = 1$, Equation (2.17) reduces to Equation (2.13), as it should.

In the VE model, $\boldsymbol{D}$ is a 4×4 matrix given by

$$\boldsymbol{D} = \begin{bmatrix} \mu_x & 0 & 0 & 0 \\ 0 & \mu_y & 0 & 0 \\ 0 & 0 & \mu_z & 0 \\ 0 & 0 & 0 & \mu_u \end{bmatrix}. \tag{2.18}$$

For two coupled oscillators, the adjacency matrix is

$$\boldsymbol{A} = \begin{bmatrix} 0 & 1 \\ 1 & 0 \end{bmatrix} \tag{2.19}$$

and hence Equation (2.17) reduces to

$$\frac{d\boldsymbol{c}_i}{dt} = \begin{bmatrix} \dot{x} \\ \dot{y} \\ \dot{z} \\ \dot{u} \end{bmatrix} + \begin{bmatrix} \mu_x & 0 & 0 & 0 \\ 0 & \mu_y & 0 & 0 \\ 0 & 0 & \mu_z & 0 \\ 0 & 0 & 0 & \mu_u \end{bmatrix} \begin{bmatrix} x_j - x_i \\ y_j - y_i \\ z_j - z_i \\ u_j - u_i \end{bmatrix} = \begin{bmatrix} \dot{x} + \mu_x \Delta x \\ \dot{y} + \mu_y \Delta y \\ \dot{z} + \mu_z \Delta z \\ \dot{u} + \mu_u \Delta u \end{bmatrix} \tag{2.20}$$

where $\Delta k = k_j - k_i$. The coefficients of diffusive transport for our system were derived using a geometric point model [41]. For our simulations, we use

$$\begin{bmatrix} \mu_x & \mu_y & \mu_z & \mu_u \end{bmatrix} = \begin{bmatrix} 0.0020 & 0 & 0 & 0.0987 \end{bmatrix} \text{ s}^{-1}. \tag{2.21}$$

In other words, diffusion is dominated by Br_2 in our system. Br_2 is readily converted into inhibitor (Br^-) via the reaction

$$Br_2 + CH_2(COOH)_2 \rightarrow Br^- + BrCH(COOH)_2 + H^+, \tag{2.22}$$

which leads to inhibitory coupling between oscillators. The effects of this will be discussed in detail in Chapter 4.

Specific geometries of interest we are studying include rings of oscillators [41] and star graphs, with geometries for a ring of six and a star graph with six nodes illustrated in Figure 2.3. Corresponding adjacency matrices for rings of N oscillators and star graphs with $(N-1)$ nodes, where the central node for the star graph is represented by droplet number 1, are

$$\boldsymbol{A}_{\text{ring}} = \begin{array}{c} \\ 1 \\ 2 \\ 3 \\ 4 \\ \vdots \\ N \end{array} \begin{array}{c} \begin{array}{cccccc} 1 & 2 & 3 & 4 & \cdots & N \end{array} \\ \begin{bmatrix} 0 & 1 & 0 & 0 & \cdots & 1 \\ 1 & 0 & 1 & 0 & \ddots & 0 \\ 0 & 1 & 0 & 1 & \ddots & \vdots \\ 0 & 0 & 1 & 0 & \ddots & 0 \\ \vdots & \ddots & \ddots & \ddots & \ddots & 1 \\ 1 & 0 & \cdots & 0 & 1 & 0 \end{bmatrix} \end{array}, \quad \boldsymbol{A}_{\text{star}} = \begin{array}{c} \\ 1 \\ 2 \\ 3 \\ 4 \\ \vdots \\ N \end{array} \begin{array}{c} \begin{array}{cccccc} 1 & 2 & 3 & 4 & \cdots & N \end{array} \\ \begin{bmatrix} 0 & 1 & 1 & 1 & \cdots & 1 \\ 1 & 0 & 0 & 0 & \cdots & 0 \\ 1 & 0 & 0 & 0 & \cdots & 0 \\ 1 & 0 & 0 & 0 & \cdots & 0 \\ \vdots & \vdots & \vdots & \vdots & \ddots & \vdots \\ 1 & 0 & 0 & 0 & \cdots & 0 \end{bmatrix} \end{array}. \tag{2.23}$$

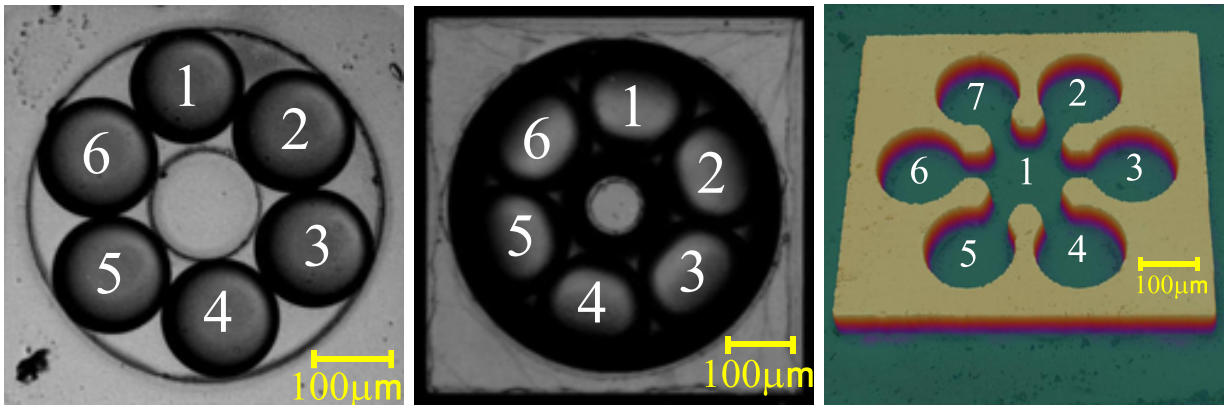

Figure 2.3: Rings of six oscillators in PDMS (left) and silicon (middle) and a star graph with 6 nodes in silicon (right).

2.4 Phase Model

While the four-variable VE model is an improvement over the seven-variable FKN in terms of computational efficiency, it can still be cumbersome for large simulations. The most efficient model would be a single-variable phase model, where each point in chemical space is mapped to a phase. That is, there exists a mapping f such that $f : \boldsymbol{c} \mapsto \theta$. We can define phase zero at any point $\boldsymbol{c}_0$ but for convenience, we define phase zero to be at an oxidation spike—a peak in the concentration of oxidized catalyst. Every other point on a periodic trajectory can be characterized by the time after passing $\boldsymbol{c}_0$ and is capped by the period T. This time is typically normalized by T or $T/2\pi$ so that it is bounded between 0 and 1 or 0 and 2π, respectively, and is known as the phase of the oscillator, illustrated in Figure 2.4. In this thesis, we consider phase that is bounded between 0 and 1; this notion of phase allows us to transform Equation (2.13) to the simple phase model

$$\frac{d\theta}{dt} = 1. \tag{2.24}$$

The solution $\theta(t) = t + \theta_0$ advances linearly in time and is periodic with period $T = 1$ in the sense that $\theta(t)$ changes by 1 after a time T.

Before proceeding, it is useful to introduce some terminology used in dynamical systems

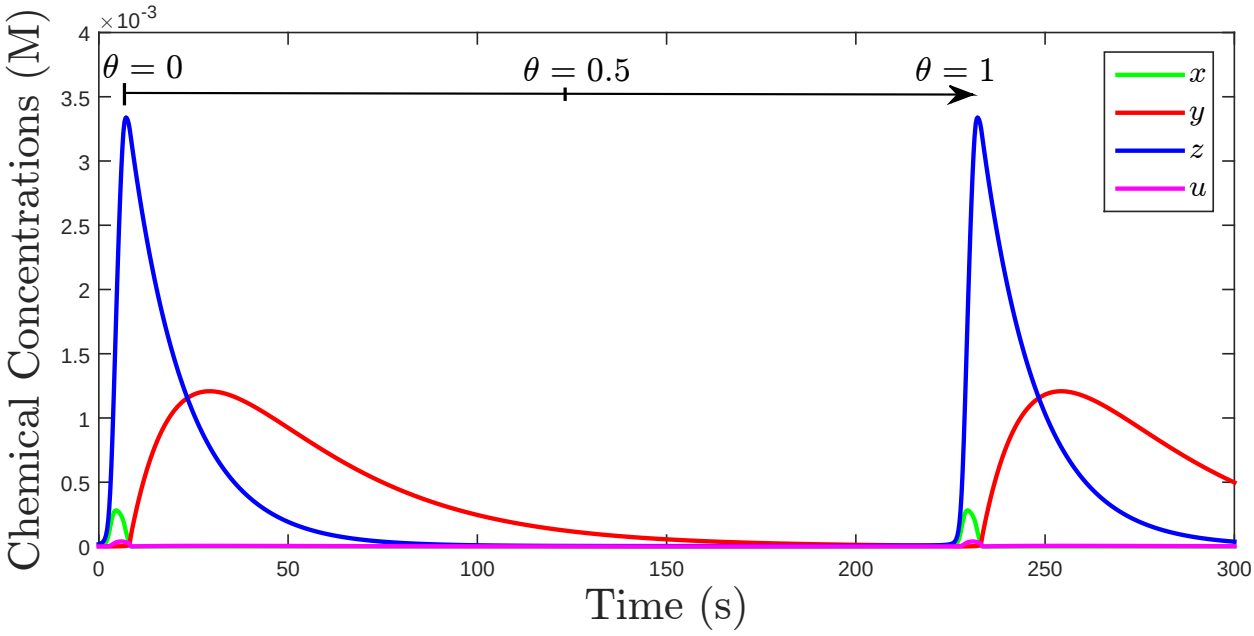

Figure 2.4: Concentrations of a BZ oscillator over one period where phase zero is defined to be at an oxidation spike.

theory. Let us begin with the limit cycle. Consider a chemical oscillator in terms of its chemical space or phase space—a space spanned by each of the n species. A trajectory in this n-dimensional space gives the oscillator's temporal behavior; each point on the trajectory describes the concentrations of the n chemical species at that time. An oscillator has a special property in this phase space: the existence of a limit cycle, a closed trajectory the system tends to. A generalization of this concept is known as an attractor—a subset of phase space a system tends to evolve toward from various initial conditions. The attractor can be as simple as an equilibrium point in, for example, a damped harmonic oscillator and as complicated as a set of points that exhibit chaotic behavior and even fractal structure [42].

In our system, once the BZ reaction reaches steady-state oscillations, the chemical concentrations evolve over time as prescribed by its attractor, in this case a limit cycle. As an example, consider the black curve parameterized by $z(t)$ and $y(t)$ plotted in Figure 2.5. This is a 2-dimensional projection of the 4-dimensional limit cycle onto the $y - z$ plane. Notice that any point near the limit cycle will be directed toward it, indicated by the slope field.

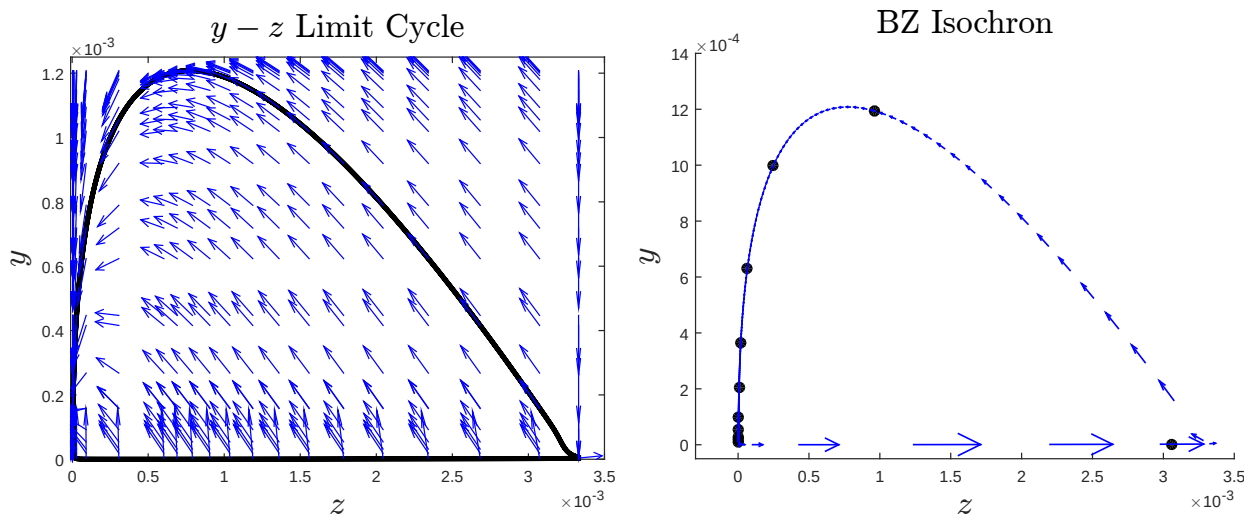

Figure 2.5: Simulated limit cycle in the $y - z$ plane. The slope field is plotted on the left while the vector field of the limit cycle's trajectory is plotted on the right. The vector field shows that the auto-catalytic oxidation is the fastest process and the decay of inhibitor and oxidized catalyst is the slowest. This is also highlighted by the ten points plotted that are equally spaced in time. The slope field shows that generally $\dot{z} < 0$ whenever $y > 0$.

Because of this, we can define the phase near a limit cycle through the notion of an isochron [8]. Consider two trajectories $r(t)$ and $s(t)$ plotted in Figure 2.6, marked by red and blue dots, respectively. The trajectory $r(t)$ is on the limit cycle while $s(t)$ is not. However, $s(t)$ eventually converges onto the limit cycle and $r(t) = s(t)$ at $t = t_4$. It is obvious that $r(t_4)$ and $s(t_4)$ can be mapped to the same phase on the limit cycle, but we can say more than that. It is also true that $s(t_3)$ and $r(t_3)$ are at the same phase since after a time $t = t_4 - t_3$, the trajectories converge to the same point. The same reasoning shows that $r(t_2)$ and $s(t_2)$ are at the same phase, and also $r(t_1)$ and $s(t_1)$. Mathematically, an isochron is a level set of the phase $\theta(t)$. The notion of an isochron is only useful if it is contained within what is known as the basin of attraction. The basin of attraction is the set in phase space such that any trajectory starting with an initial condition in the basin will eventually be directed toward the basin's (single) attractor.

This last restriction implies that a phase model is only a good approximation when there is a weak external perturbation. If, for example, a perturbation is strong enough to push an

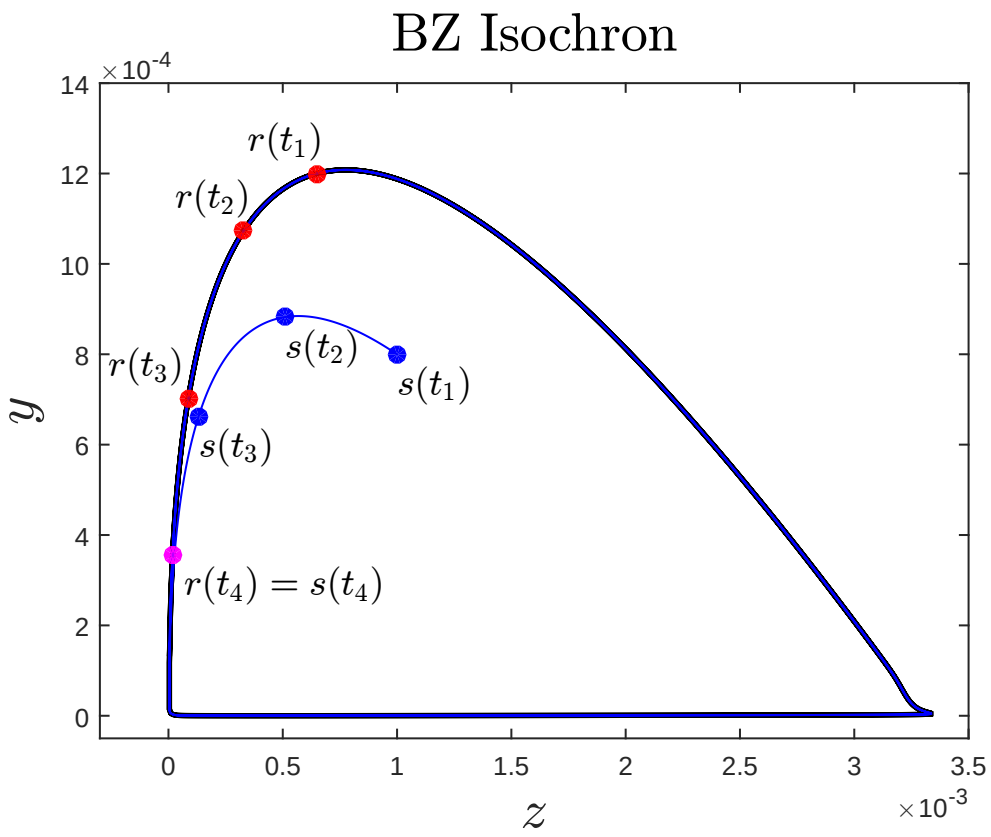

Figure 2.6: Representation of points off the limit cycle that have identical phases, constituting part of an isochron. The trajectory $r(t)$ is on the limit cycle while the trajectory $s(t)$ is off the limit cycle but they have points at times $t_1, \ldots, t_4$ with identical phases.

oscillator outside the basin of attraction, then the entire dynamics will change and the phase will no longer be an accurate representation. With this new understanding of dynamical systems, we would like to cast the n-variable model for coupled oscillators, Equation (2.17), into a simple one-variable phase model. To do this, first let us consider a single oscillator subject to a weak external time-dependent perturbation on each of the n state variables (chemical concentrations, in our case) of the form $\boldsymbol{p}(t) = [p_1(t), \ldots, p_n(t)]$. Then

$$\frac{d\boldsymbol{c}}{dt} = \boldsymbol{R}(\boldsymbol{c}) + \epsilon \boldsymbol{p}(t) \tag{2.25}$$

where ϵ is small. In our BZ system, this perturbation can be a light pulse or diffusion from neighboring oscillators. Recall that without an external perturbation, the phase model is

given by Equation (2.24). With a perturbation, it is possible to show that the phase model takes the form

$$\frac{d\theta}{dt} = 1 + \epsilon \boldsymbol{Q}(\theta) \cdot \boldsymbol{p}(t) \tag{2.26}$$

where $\boldsymbol{Q}(\theta) = [Q_1(\theta), \ldots, Q_n(\theta)]$ is the infinitesimal phase response curve (iPRC) that describes the instantaneous change in frequency in response to a perturbation to all state variables [8]. It is obtained by linearly scaling the phase response curve (PRC, discussed in detail in Chapter 4, Section 4.6), which is valid for weak perturbations such that

$$\mathrm{PRC}(\theta, A) \approx Q(\theta)A. \tag{2.27}$$

To measure it, we must weakly perturb each state variable and then take the limit

$$Q(\theta) = \lim_{A \to 0} \frac{\mathrm{PRC}(\theta, A)}{A} = \left. \frac{\partial \mathrm{PRC}(\theta, A)}{\partial A} \right|_{A=0}. \tag{2.28}$$

Since we are interested in modeling coupled oscillators, let us consider a perturbation on the i-th oscillator from its neighbors of the form

$$\boldsymbol{p}_i(t) = \sum_{j=1}^{N} A_{ij} g_{ij}(\boldsymbol{c}_i, \boldsymbol{c}_j), \tag{2.29}$$

where g_{ij} describes the interaction between oscillators i and j. Mapping the concentrations to phase, that is $\boldsymbol{c}_i \mapsto \theta_i$, we can write the phase model as

$$\begin{aligned} \frac{d\theta_i}{dt} &= 1 + \epsilon Q_i(\theta_i) \sum_{j=1}^{N} A_{ij} g_{ij}(\theta_i, \theta_j) \\ &= 1 + \epsilon \sum_{j=1}^{N} \boldsymbol{H}(\theta_i, \theta_j), \end{aligned} \tag{2.30}$$

where the entries of $\boldsymbol{H}$ are $h_{ij} = Q_i A_{ij} g_{ij}$. The function $\boldsymbol{H}$ is known as the generalized coupling function and describes the interactions between a network of oscillators in terms of their phases. In principle, once $\boldsymbol{H}$ is measured the system can be described by a single variable. In practice, however, $\boldsymbol{H}$ is difficult to measure because one must account for the

effects of a weak perturbation in each state variable and measure the infinitesimal phase response curve to perturbation. Despite these complications, this generalized phase model has described synchronization in a large collection of coupled oscillators, including networks of neurons [43, 44]. One special case of Equation (2.30) has a coupling function that depends on the sine of the phase difference,

$$\frac{d\theta_i}{dt} = \omega_i + \frac{K}{N}\sum_{j=1}^{N}\sin(\theta_j - \theta_i), \tag{2.31}$$

where ω_i is the natural frequency of each of the N oscillators and K is a constant describing the interaction strength. It is known as the Kuramoto model and assumes global weak coupling and nearly identical oscillators with a small spread in natural frequencies. It turns out that the Kuramoto model can be solved analytically in the $N \to \infty$ limit and has been used to describe synchronization in biological and chemical systems, with applications to neuroscience and even coupled Josephson junctions [1, 45].

Chapter 3

Experimental Methods

3.1 BZ Recipe

Our BZ recipe consists of the six reactants with associated final concentrations listed in Table 3.1. We prepare the reactants in two distinct eppendorf tubes so that the reaction does not start until droplet formation. The medium separating droplets is a fluorinated oil (HFE 7500) that is stabilized by surfactant (EA) so that the droplets do not coalesce [46]. Moreover, Br_2 is quite hydrophobic and diffuses into hydrocarbons easily, including the fluorinated oil [47]. This establishes the predominantly inhibitory coupling we observe.

Table 3.1: Separation of BZ reactants into two tubes with their final concentrations.

Tube 1		Tube 2	
Reactant	Concentration	Reactant	Concentration
Malonic Acid	400 mM	Sodium Bromate	300 mM
Sulfuric Acid	80 mM	Ferroin	3 mM
Sodium Bromide	2.5 mM	$Ru(bipy)_3$	1.2 mM

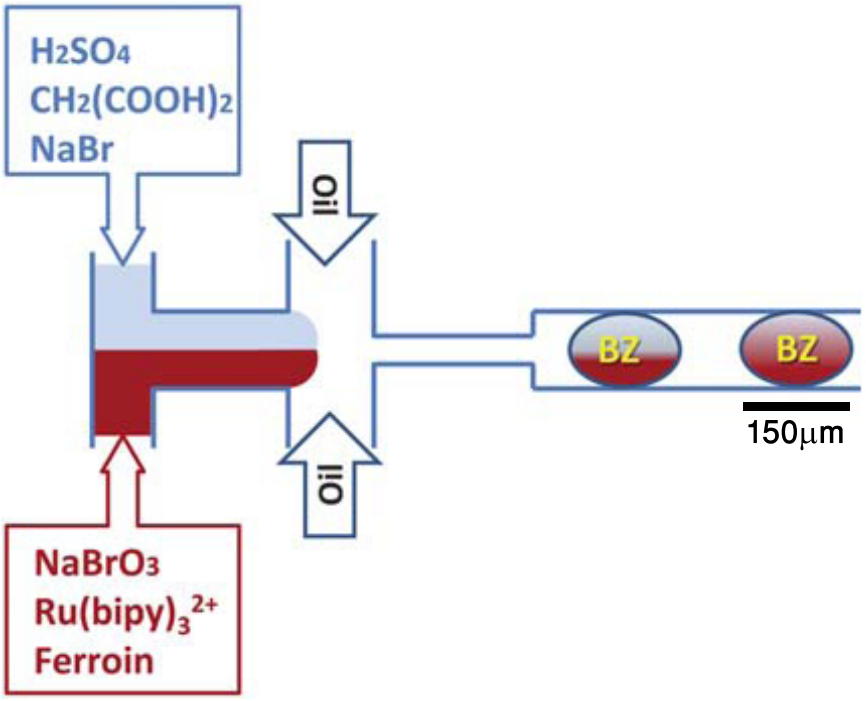

Figure 3.1: Schematic of a flow-focusing PDMS chip used to generate BZ droplets. Two complementary streams of BZ merge and co-flow until pinched by perpendicular streams of oil, resulting in the formation of droplets. Adapted from [48].

3.2 Micro-droplet Production

To produce a BZ emulsion, we use a flow-focusing polydimethylsiloxane (PDMS) chip whose key components are sketched in Figure 3.1 [48]. It consists of two streams of BZ with reactants separated as in Table 3.1 to prevent the reaction from starting until droplets are formed. The BZ streams meet and co-flow until they are met by two perpendicular streams of oil that generate the droplets [49]. Our droplets are typically on the order of 100 μm in diameter and have nanoliter volume. Because of their small size ($d \approx 100$ μm) and the relatively fast rate of diffusion of aqueous species ($D \approx 10^{-5}$ cm^2/s $= 10^3$ μm^2/s), the characteristic time of diffusive mixing inside a droplet is

$$\tau_D = d^2/D \approx 10 \text{ s}, \tag{3.1}$$

which is much less than the 250–350 s period of oscillation [47]. As a result, we may approximate the concentrations within each droplet to be homogenous, which validates the chemical homogeneity assumption in our model of coupled oscillators (Assumption 1, Section 2.3).

The flow rates for each channel typically range from 300 to 600 μL/hr. Various combinations yield different sized droplets. The droplets used in this thesis are all roughly 150 μm in diameter, generated by a 500 μL/hr oil flow rate and a 400 μL/hr flow rate in each of the BZ streams. Increasing (decreasing) the oil flow rate decreases (increases) the droplet size, and increasing (decreasing) the BZ flow rate increases (decreases) the droplet size.

We export the droplets into a third eppendorf tube and load them via capillary action into a rectangular borosilicate glass capillary (VitroTubes$^{\text{TM}}$) with an inner diameter of 100 μm, slightly smaller than the droplet diameter. The result is a close-packed emulsion of droplets as shown in Figure 3.2. We place the capillaries on a glass slide and use commercial 5-minute quick-cure epoxy (Bob Smith Industries) to seal both edges to prevent air from leaking in.

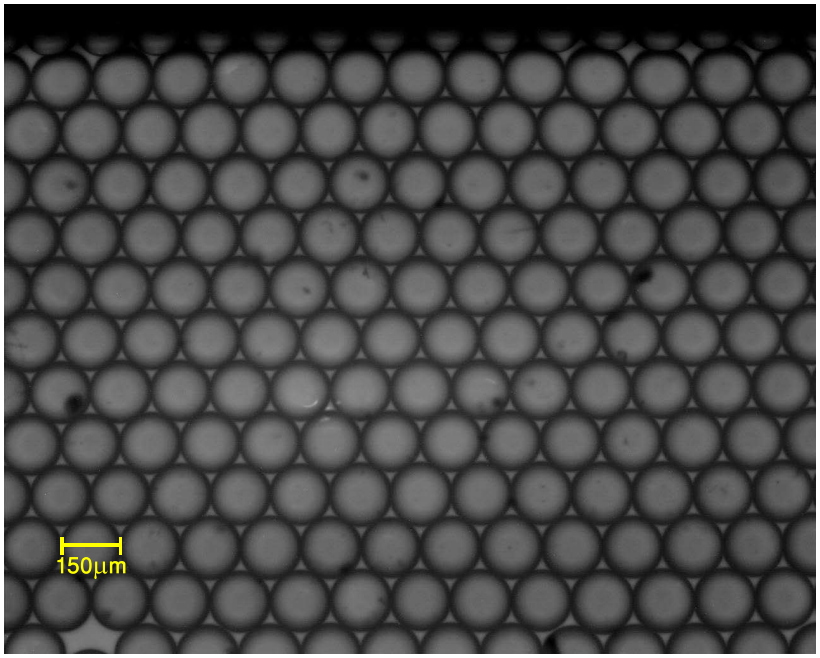

Figure 3.2: Image of a close-packed emulsion of 150 μm diameter BZ droplets separated by thin oil gaps in a rectangular glass capillary with an inner diameter of 100 μm.

3.3 Programmable Illumination Microscope

We image and project programmable illumination onto our BZ droplets using a custom built Programmable Illumination Microscope (PIM) [50]. A schematic of the optics is displayed in Figure 3.3. It consists of a commercial three-color liquid-crystal display (LCD) projector with the optics inverted so that it focuses inward rather than projecting outward. It is coupled with MATLAB code that is able to detect, track, and project light onto individual 150 μm droplets.

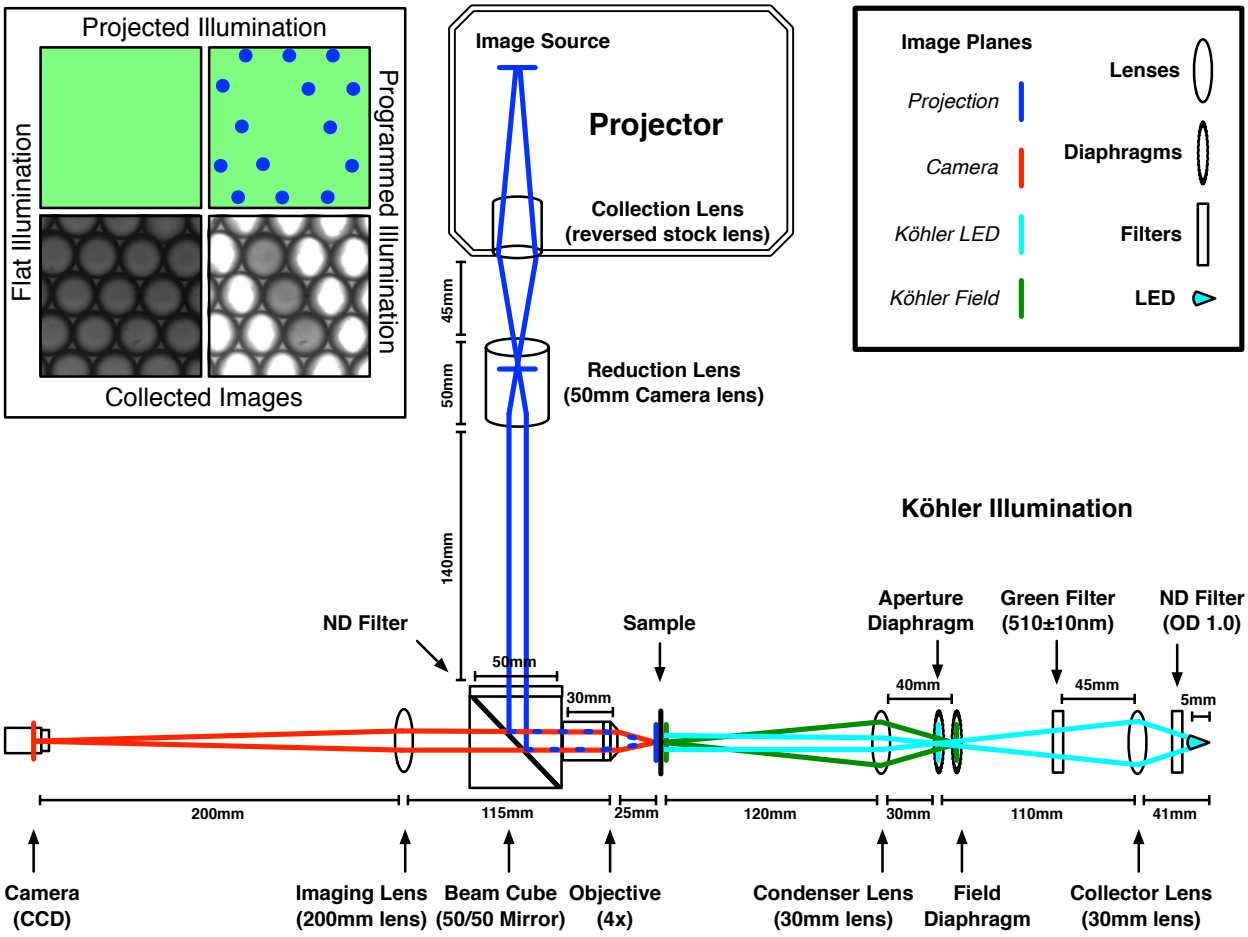

Figure 3.3: Schematic of the optics in our Programmable Illumination Microscope. It consists of a commercial projector with inverted optics that projects blue light onto the sample, which is illuminated by green Köhler illumination on the right arm. Images are taken by a CCD on the left arm. An example of projected light on a sample is shown in the top-left.

Two representative images before and after projected light are shown in the top-left of Figure 3.3. We project blue light with wavelength $\lambda \approx 452$ nm such that it excites the $Ru(bipy)_3$ and as a result can inhibit oscillations in particular droplets as discussed in Chapter 2, Section 2.1. We can change the size and intensity of the projected dots; varying these parameters alters the behavior of BZ droplets as will be discussed in Chapter 4. To illuminate our sample, we can project flat illumination in addition to the blue dots on each individual drop. This is useful if the sample is not transparent, but because we place our drop-containing capillaries on a glass slide, we can also image our sample with a more uniform Köhler illumination using a cyan LED and a green filter that filters light of wavelength $\lambda = 510 \pm 10$ nm. We use green light to image our sample because it does not excite $Ru(bipy)_3$ and moreover, allows us to capture the oxidation spike due to the color change from red (ferroin) to blue (ferriin). This is because green light is absorbed by ferroin and transmitted through ferriin [41], so droplets appear bright in the oxidized state and dark in the reduced state when imaged by a black-and-white CCD, as seen in Figure 3.4.

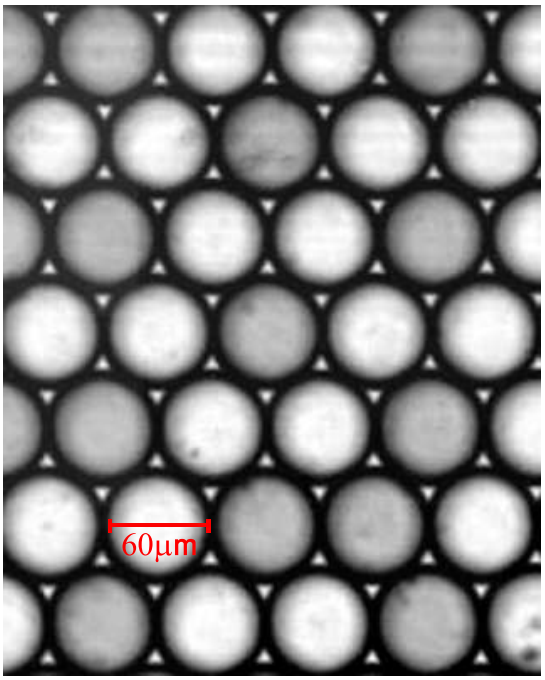

Figure 3.4: Image of BZ droplets highlighting the difference between droplets in the oxidized state (brighter) and reduced state (darker). From [41].

We take an image every 10 seconds and record in real-time when oxidation spikes occur. Droplets are in the oxidized state for roughly $0.1\,T_0$ where T_0 is the measured natural period. Since typically 250 s $< T_0 <$ 350 s, the oxidation spikes are always captured. The time between spikes gives us the periods of each droplet and hence we can linearly interpolate between spikes to assign previous phases and predict future phases. Furthermore, the variation in the period difference from measurement to measurement is only 8 ± 10 s $\approx 0.02T_0 \pm 0.03T_0$. This allows us to accurately predict future phases of oscillation and use algorithms that perturb desired oscillators via light pulses at pre-programmed phases. Experiments that do this will be discussed in Chapter 4 and Chapter 5.

Our resolution is limited to 10 seconds between images because of the calculation time needed to detect and track over 100 droplets, compute quantities of interest, and align projected light [50]. This also presents a second problem in that light can not be projected while these calculations are being performed. As a result, we cannot shine truly constant light, but rather pulsed light that has a 30% duty cycle; the light is on for 3 seconds and then off for 7 seconds. However, because the frequency of oscillation is so much smaller than the frequency of pulsed light, as shown in Figure 3.5, we can treat the light to be effectively constant but at reduced intensity. More justification will be given in Chapter 4, Section 4.5.1 after describing the effects of (high frequency) pulsed light in a few experiments.

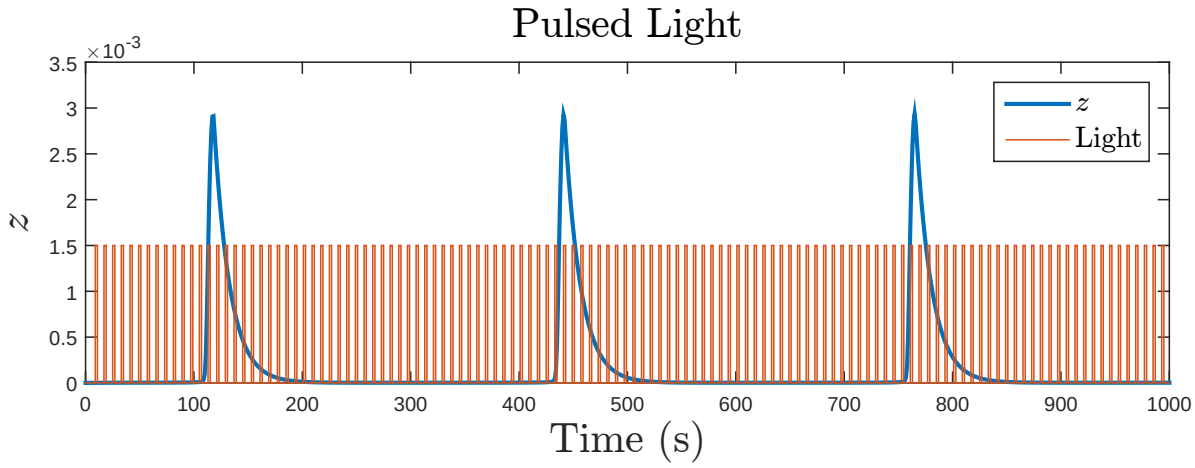

Figure 3.5: Oscillations in z with pulsed light overlayed at a 30% duty cycle (3 s on, 7 s off).

Chapter 4

Synchronization Engineering

An important, relevant example of synchronization occurs in networks of neurons in the brain where the synchronization can lead to macroscopic oscillations. The networks comprising these oscillations are called central pattern generators which, when activated in the absence of sensory feedback, have been shown to produce rhythmic motor patterns like walking, breathing, flying, and swimming [51]. Synchronization of oscillators has also been shown as a fundamental mechanism for combining and relating information to different areas of the brain. Moving toward the pathological, neuronal synchronization has been shown to contribute to tremors and seizures [52].

Synchronization engineering has been used in deep brain stimulation for patients suffering from Parkinson's disease by implanting electrodes [52] and in treating cardiac arrhythmia [53]. Mathematical descriptions in the form of phase models have been constructed to describe systems of weakly coupled oscillators and to tune them to desired states [54]. We are interested in experimentally characterizing the attractors for various networks of BZ oscillators and discovering and implementing algorithms to transition from attractor to attractor via optical perturbations. We hope this will further our understanding of networks of coupled oscillators and allow us to create synthetic, controllable central pattern generators capable of operating chemomechanical BZ gels.

In this chapter, we discuss the effects of inhibitory coupling between BZ oscillators that give us intuition as to what the expected attractors are. We also discuss the effects of optical perturbations that will set up a framework for synchronization engineering.

4.1 Inhibitory Coupling

The steady-state configuration of two coupled oscillators provides the simplest example of synchronization. Two BZ oscillators coupled via inhibition tend to synchronize anti-phase—that is, they oscillate 180 degrees out of phase. We call this the anti-phase attractor. To understand this, consider two identical coupled coupled oscillators that begin slightly out of phase, as shown in Figure 4.1.[1] Recall that the concentration of Br_2 follows the concentration of ferriin (Figure 2.2). As a result, Br_2 is at a maximum concentration near oxidation spikes and diffuses into neighboring drops. The blue drop, due to its shorter period, spikes first and thus Br_2 diffuses into the green drop before it spikes. The Br_2 is then converted to inhibitor Br^- (Equation 2.22). This effect is amplified after each successive oscillation until eventually the green drop is delayed half a period where the two oscillators remain by symmetry since diffusion is bi-directional, as shown in Figure 4.2.

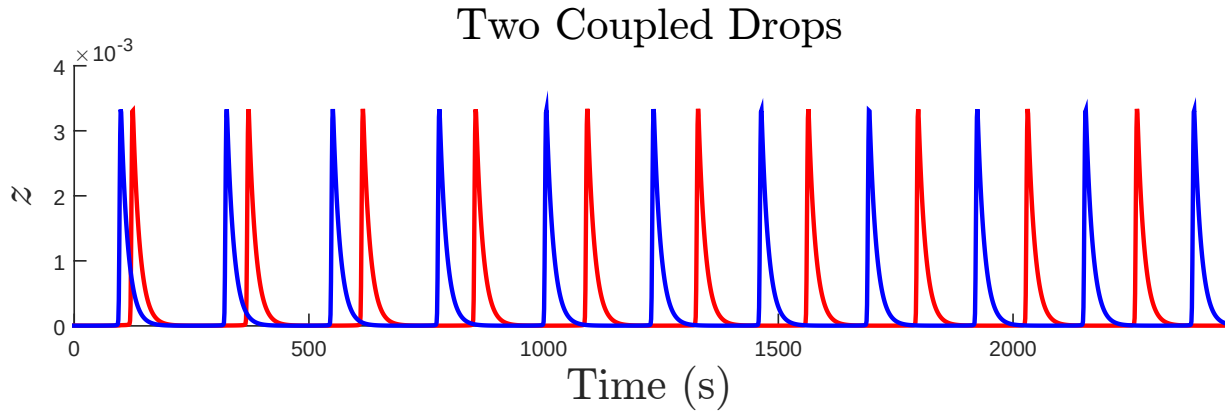

Figure 4.1: Oscillations of two initially in-phase oscillators coupled via inhibition with slightly different periods. They eventually drift apart and remain at the anti-phase attractor.

[1]Note that if the oscillators started in phase, they would remain there, constituting a second attractor. However, this rarely happens in practice due to heterogeneities in nature.

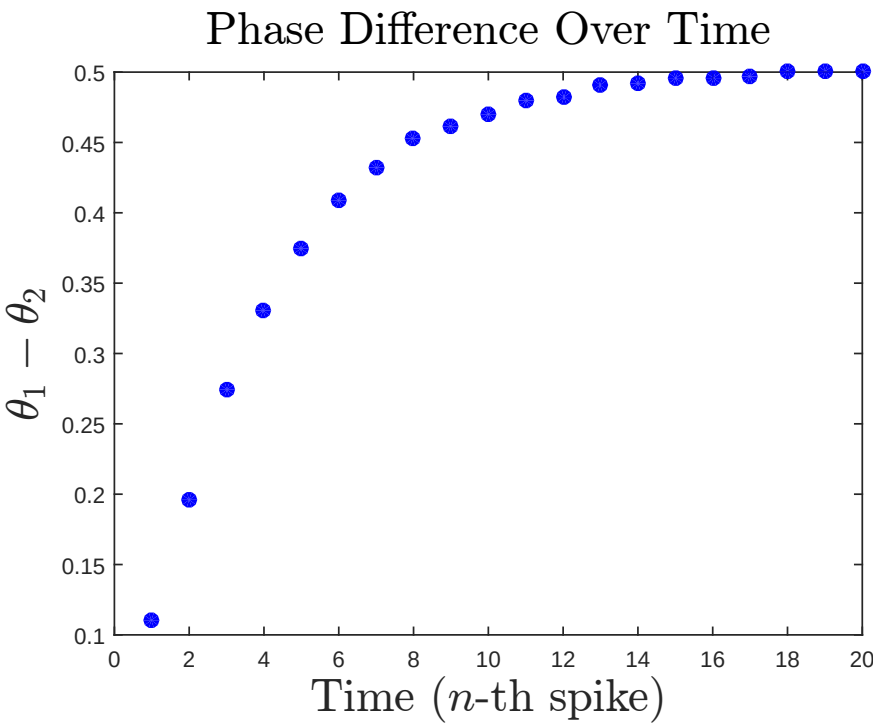

Figure 4.2: Phase difference as a function of time between two coupled oscillators via inhibition. The oscillators begins lightly out of phase and the phase difference grows to 0.5.

For a one-dimensional array of oscillators, the anti-phase attractor remains, where every oscillator tends to align 180 degrees out of phase with its neighbors [47]. In two-dimensional rings, we again observe the anti-phase attractor for an even number of members [41]. However for a ring with an odd number of members, it is impossible for them to all oscillate 180 degrees out of phase. In this case, there is a $(N-1)/2N$ phase separation between drops, which results in N phase clusters separated by $1/N$. We also observe stationary patterns as the coupling strength between droplets increases by varying the chemistry and decreasing drop size [41].

4.2 Optical Perturbations

To develop an intuition for the effects of optical perturbations, we turn to the VE model (Equations 2.9 through 2.12). For constantly applied light with low rates of $Ru(bipy)_3$

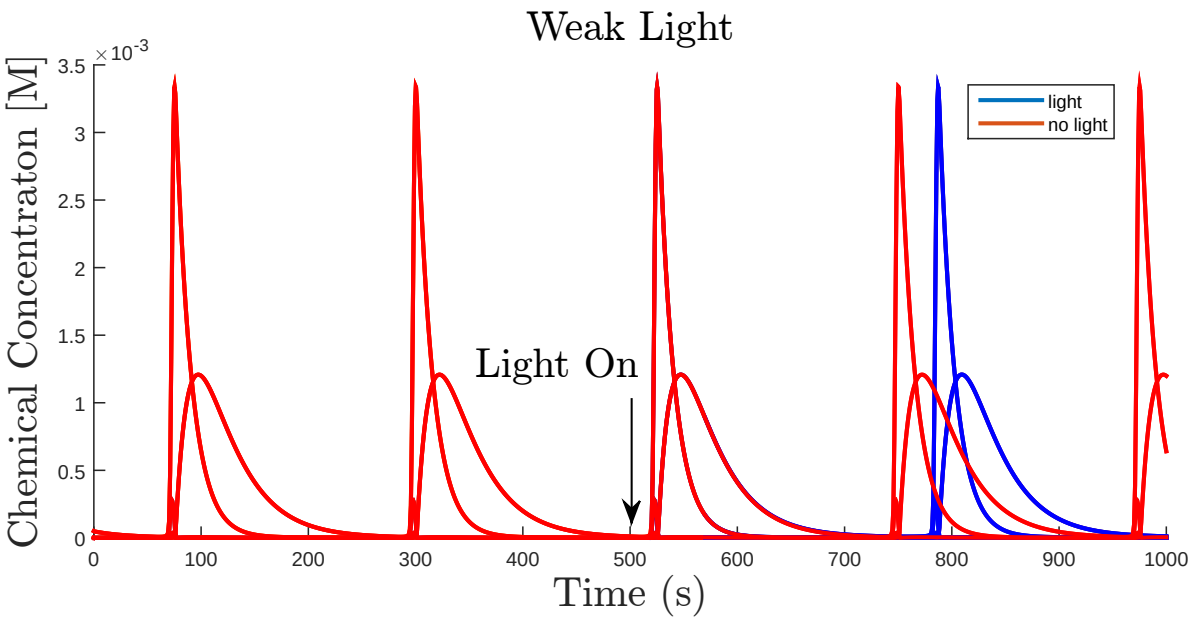

Figure 4.3: Simulation of the four chemical concentrations for two curves, red and blue, with the same initial parameters. The red curves are reference curves with no light applied and the blue curves are optically perturbed weak, constant light ($k(I) < k(I_c)$) at $t = 500$ s. They overlap initially, as expected, but the blue curves deviate slightly after light is applied. The effects ares most noticeable after one full period, delaying the blue oxidation spike.

excitation, $k(I)$, the additional inhibitor introduced delays the oxidation spike as shown in Figure 4.3. Plotting only the concentration of inhibitor in Figure 4.4 shows slight deviations from the perturbed and unperturbed trajectories. In particular near $t \approx 630$ s, the perturbed trajectory begins to have noticeably more inhibitor in the system, highlighted by the zoomed in snapshot. This is because the (constantly) applied light effectively adds a constant amount of inhibitor, y, to the system. Thus, when the rate of change of y is large, the effect is negligible. However toward the end of the oscillation ($\theta \approx 0.7$), the decay rate of y is slowest and hence a constant addition has the largest effect.

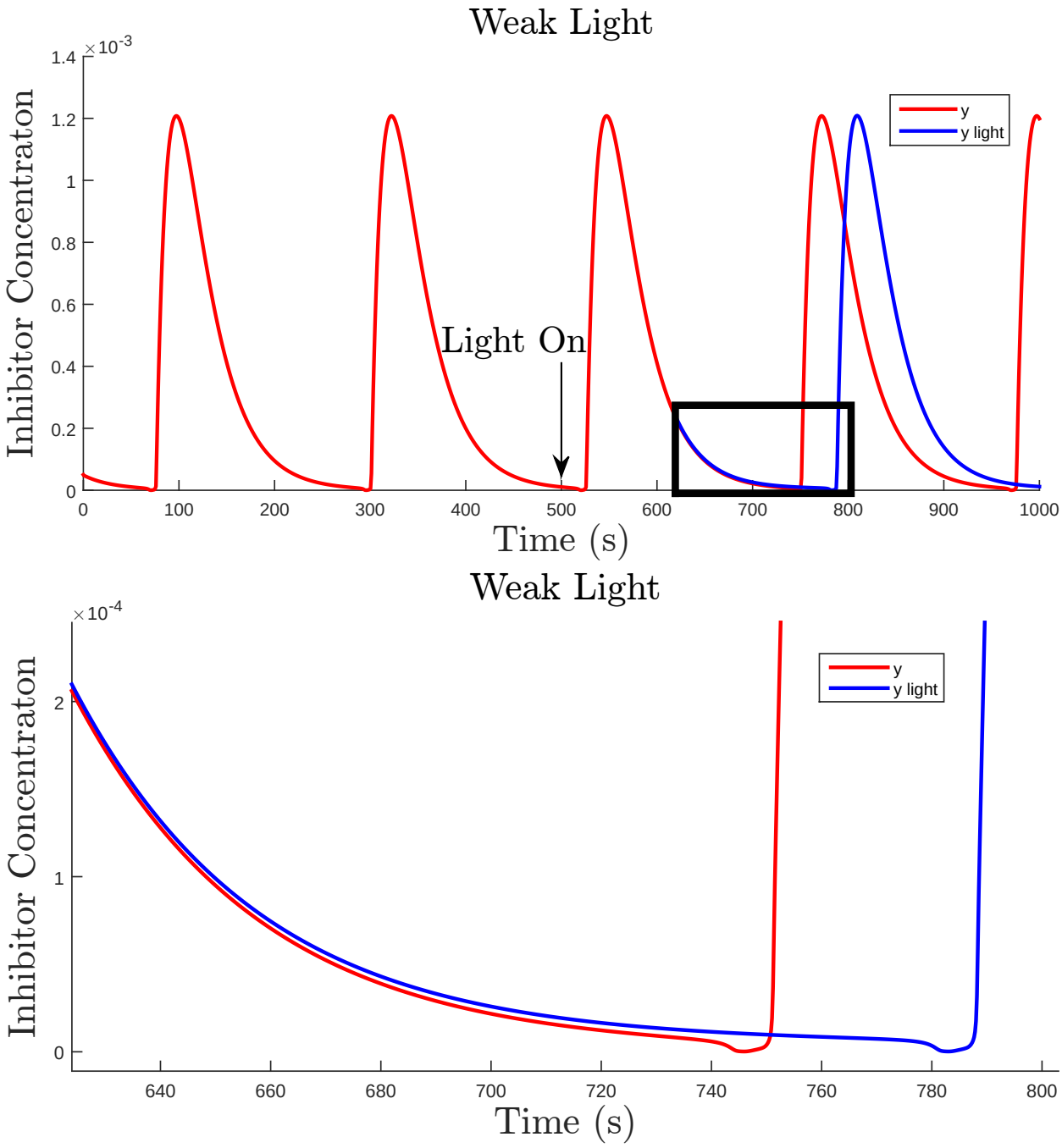

Figure 4.4: Simulation as in Figure 4.3 but only plotting inhibitor. The bottom half is a zoomed in snapshot of the section marked by the black rectangle. The constant addition of inhibitor in the perturbed trajectory becomes noticeable when the rate of decay is low, hence delaying the oxidation spike.

As $k(I)$ is increased, more and more photo-sensitive catalyst is excited and hence oxidized, generating more inhibitor (Equation 2.7). There reaches a critical intensity I_c such that $k(I) = k(I_c)$ is so fast that the inhibitor never fully decays and oscillations cease as shown in Figure 4.5. After initial transients following applied light, the concentrations of all four chemical species approach a constant. Zooming in near $t = 800$ s, we see that indeed x, y, z and u are constant, where the black dotted lines are horizontal lines for reference. Increasing the intensity above the critical threshold increases the constant-chemical concentrations as demonstrated in Figure 4.6. The most noticeable effect is on inhibitor, y. The concentration of catalyst z increases significantly in the model because it consists of only one photo-sensitive catalyst; there is no ferroin.

In summary, the model predicts that low intensities of light, resulting in slow excitation rates $k(I)$, elongate the period of BZ oscillators and there is a critical intensity of light that prevents oxidation spikes and hence oscillations entirely. The rest of this chapter discusses experiments that demonstrate the properties mentioned above.

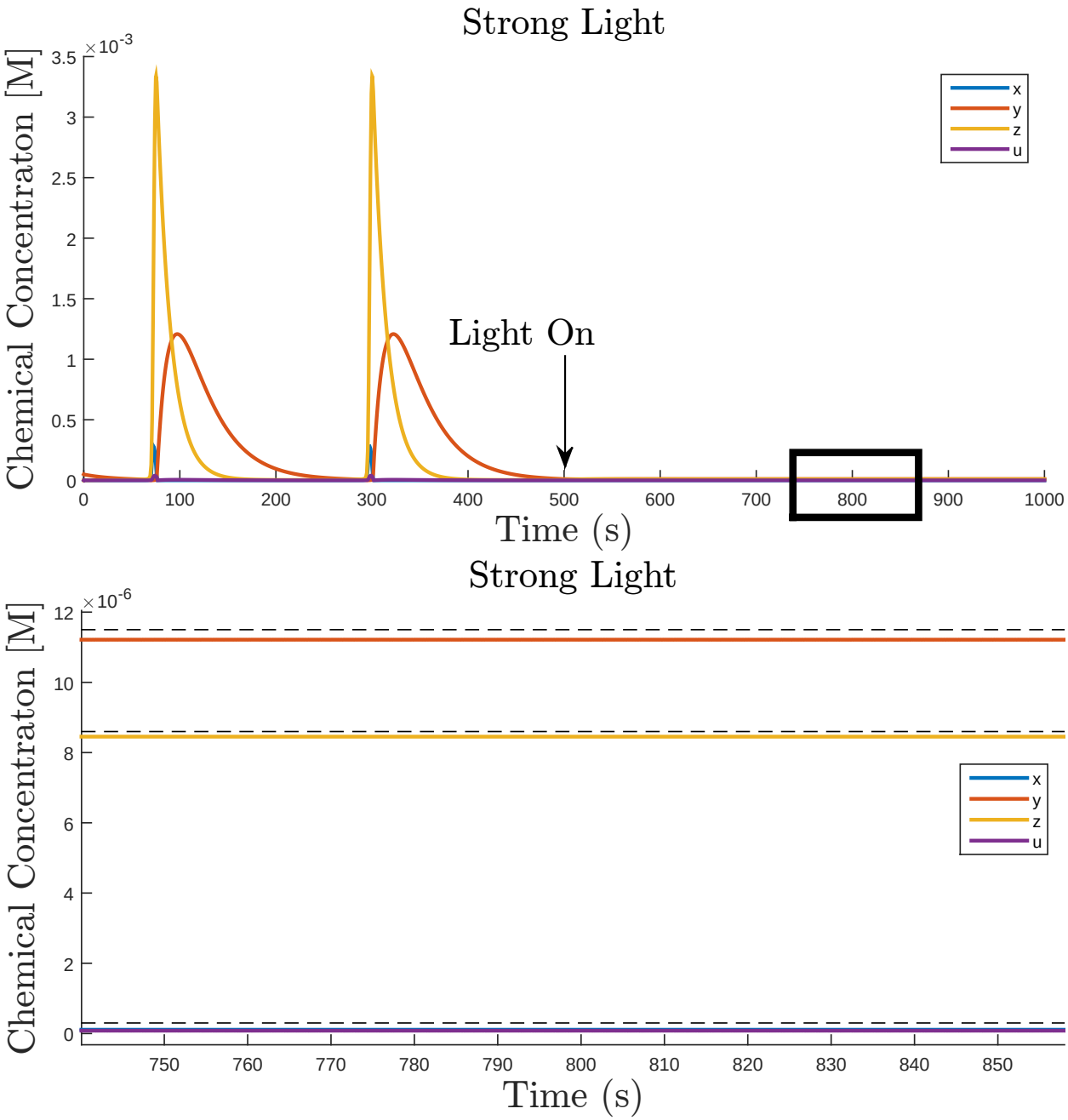

Figure 4.5: Simulation of the four chemical concentrations optically perturbed with strong, constant light ($k(I) > k(I_c)$) at $t = 500$ s. All oscillations cease due to rapid production of inhibitor. Eventually the chemical concentrations reach a constant value indicated by the bottom half of the figure, with constant dotted horizontal lines for reference.

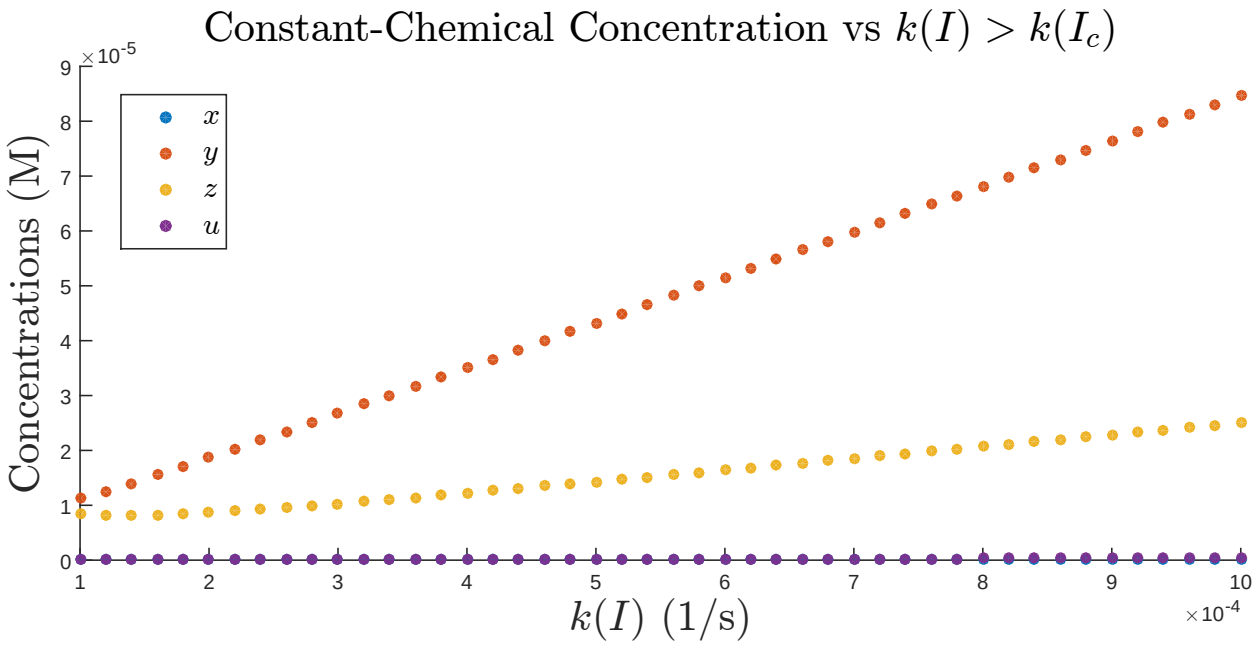

Figure 4.6: Simulation of the four chemical concentrations as a function of $k(I)$ above the critical threshold for suppression of oscillations. The constant-chemical concentrations increase at higher intensities since more photo-sensitive catalyst is oxidized (including x and u, though they increase at a far slower rate).

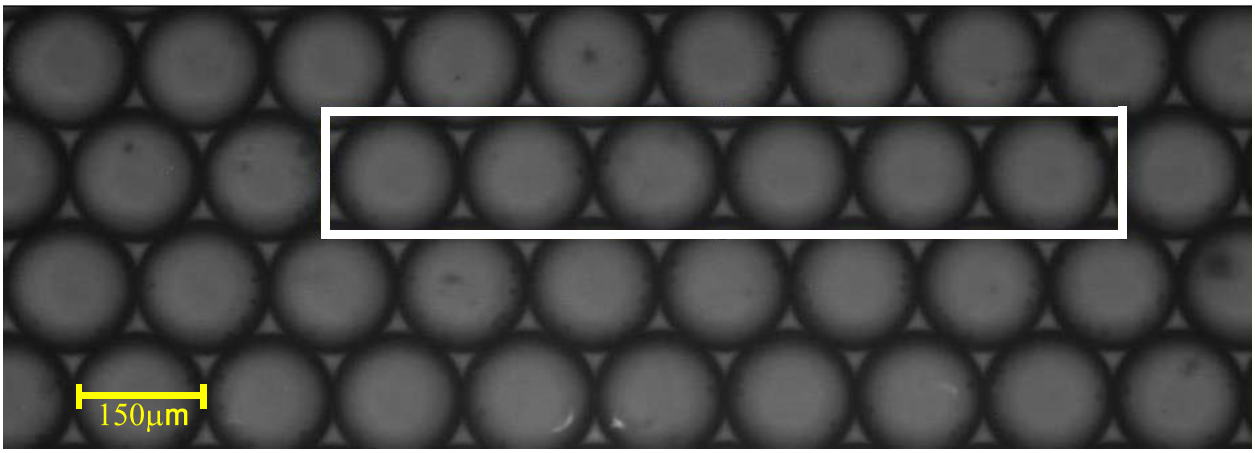

Figure 4.7: Image of an emulsion of 150 μm diameter BZ droplets separated by thin oil gaps in a rectangular glass capillary. The boxed droplets are used to construct the space-time plot in Figure 4.8.

4.3 Control Over Initial Conditions

Adding a photo-sensitive catalyst, $Ru(bipy)_3$, to the reaction allows blue light at sufficiently high intensities to force the reaction into a constant-chemical state. To verify this property, we created a 2D emulsion of 150 μm diameter BZ droplets separated by thin oil gaps such that they are coupled via inhibition, as shown in Figure 4.7. We projected light on the entire sample, removed the light, and observed the resultant behavior. To obtain information regarding the oscillations of each droplet over time, we created a space-time plot as shown in Figure 4.8. It is obtained by digitizing the pixel intensities along a slice through the center of the boxed droplets in Figure 4.7, illustrated by the red line through the (contrast-enhanced) droplets in Figure 4.8a. These intensities are then plotted as a function of time in Figure 4.8b. The narrow bright lines in the space-time plot correspond to oxidation spikes.
We can use this information to measure relative phases at any given time. For example, the space-time plot tells us that the six droplets all initially oscillate in-phase.

It is possible to re-synchronize the oscillators by illuminating them with light again as indicated in Figure 4.8b, which resets them to be in the same constant-concentration state. All oscillations cease while light is on and the droplets again oscillate in-phase shortly after light is removed. This ability to synchronize droplets at will is useful to set in-phase initial conditions and can also in theory be used to initialize any set of initial conditions by removing light on particular droplets at selected times. This property will allow us to search for various attractors in a multistable network of oscillators by initializing them in different areas of phase space, which may correspond to distinct basins of attraction.

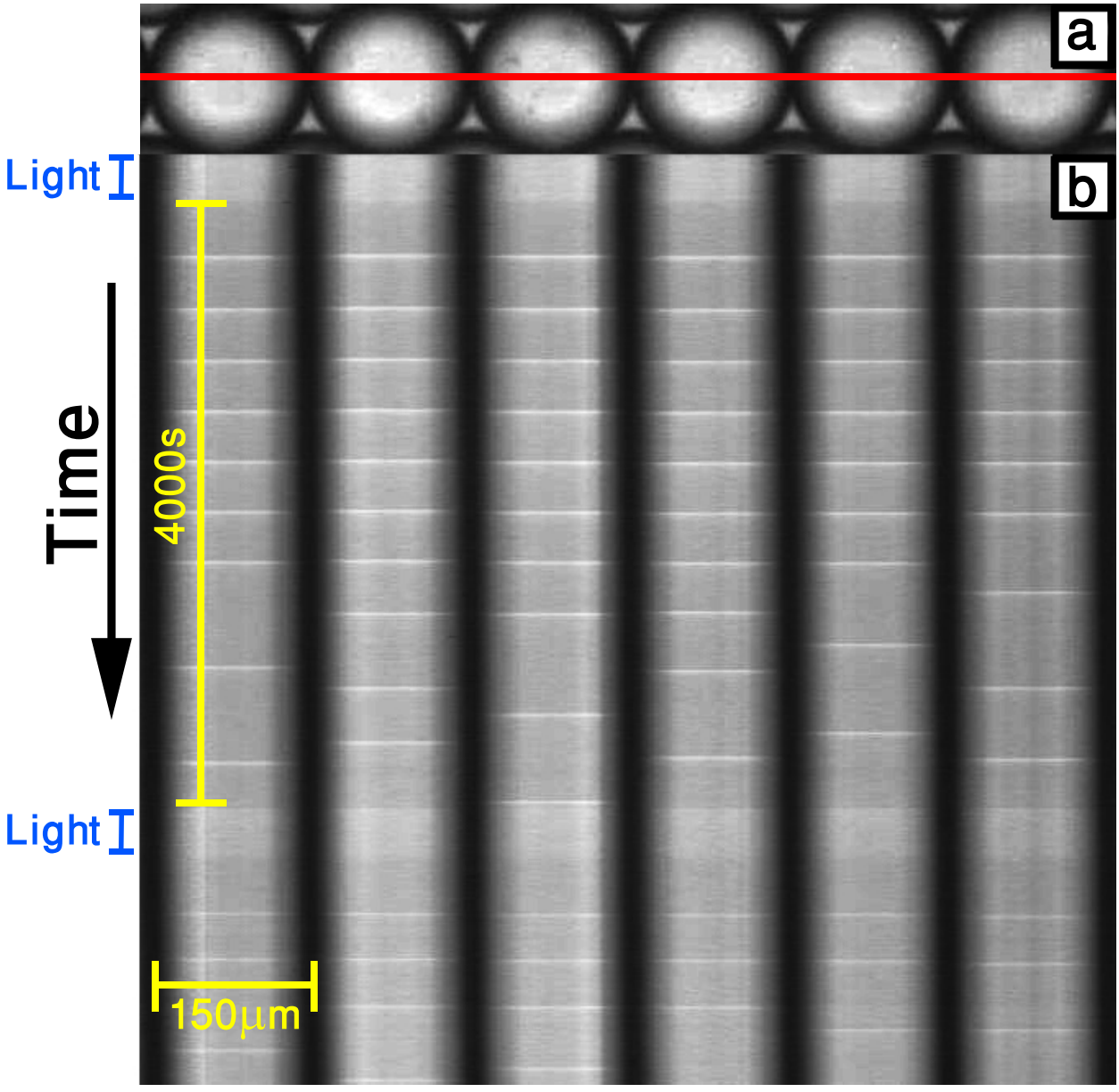

Figure 4.8: Space-time plot demonstrating the ability to set droplets in-phase using blue light. (a) The six droplets (taken from those boxed in Figure 4.7) used to generate the space-time plot by digitizing pixel intensities along the red slice. (b) Space-time plot comprised of digitized intensities as a function of time. Narrow bright lines correspond oxidation spikes.

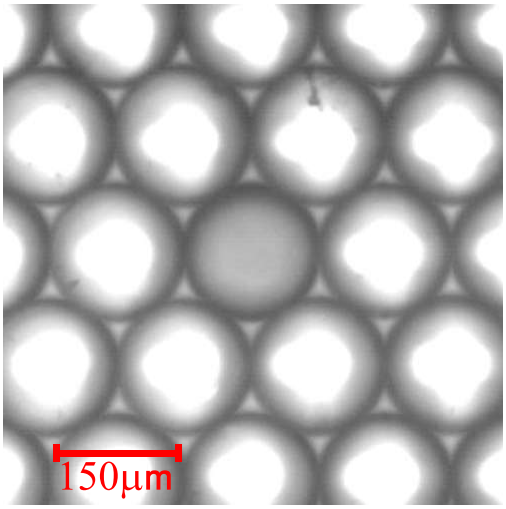

Figure 4.9: Constant-chemical boundary conditions for a single optically isolated droplet. The center droplet is free to oscillate but its neighbors are suppressed via spots of projected light.

4.4 Constant-concentration Boundary Conditions

Light perturbations can be used to not only reset phase, but also to engineer particular droplet geometries. The simplest geometry is an isolated droplet, shown in Figure 4.9. A spot of light is projected on all but the center droplet, forcing them to a constant-chemical concentration, non-oscillatory state while the chemical concentrations of the center droplet are free to oscillate.

These optically-induced boundary conditions are not equivalent to a completely isolated droplet, however. This is because the boundary droplets, though suppressed, still result in diffusion of non-polar chemical species through the oil into the center droplet. In particular, Br_2 diffuses through and is readily converted into the inhibitor, Br^-. A plot of steady-state Br_2 concentration, u, as a function of $k(I)$ above the critical threshold is shown in Figure 4.10. The concentration increases at higher $k(I)$ and is greater than the minimum concentration present with no projected light. Thus, these boundary conditions tend to elongate the period due to weak inhibitory coupling from neighbors. A second difference may be the reflection and refraction of light from the boundaries that transmit through the center droplet, which further lengthens the period.

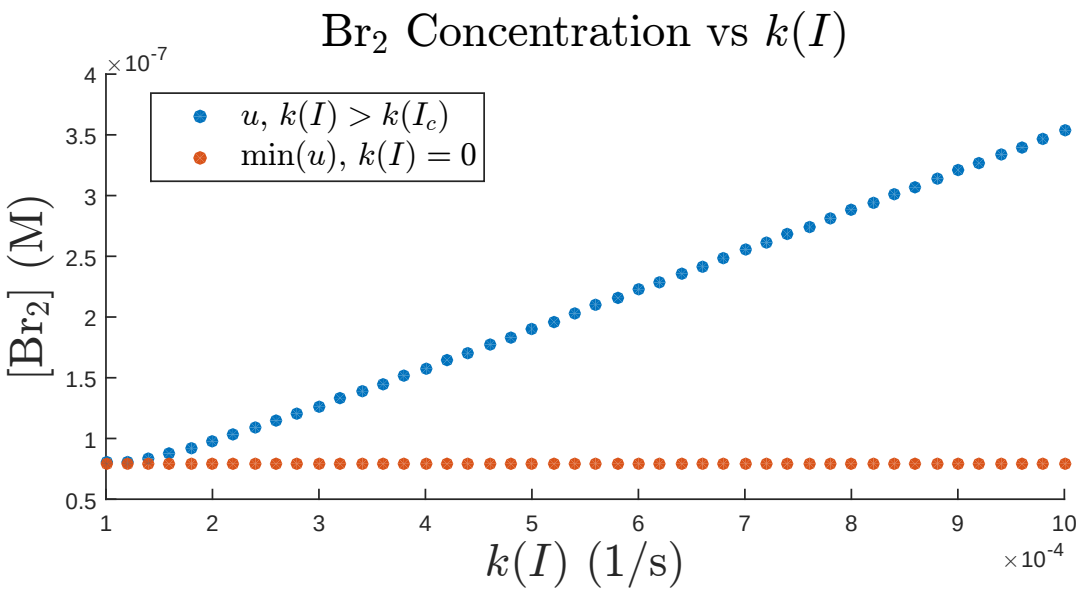

Figure 4.10: Simulation of steady-state Br_2 concentrations as function of $k(I) > k(I_c)$ the rate of excitation of $Ru(bipy)_3$, above the critical threshold for suppression of oscillations. The constant-chemical concentration increases at larger $k(I)$, which is also greater than the minimum concentration of u for a reference curve with no light applied.

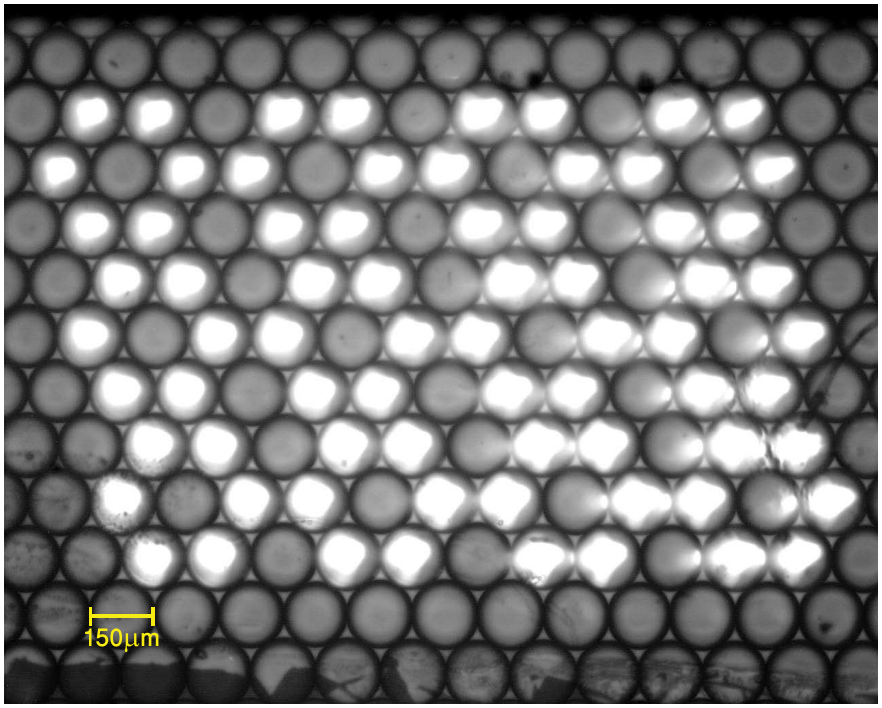

Figure 4.11: Image taken during an experiment varying the light intensity on boundary droplets and measuring the period of the central droplet. Light intensity is lowest on top left, greatest on bottom right.

To investigate the effects of intensities of light above the critical threshold, we varied the light intensity on boundary droplets, as shown in Figure 4.11, and measured the period of oscillation. A plot of period as a function of light intensity on boundary droplets in Figure 4.12 shows that the period increases considerably. It is interesting to note that it is approximately linear, as is the increase in Br_2 concentration (Figure 4.10). The intensities are scaled by the critical intensity of light, I_c, that completely suppresses oscillations of boundary droplets. Similarly, the periods are scaled by the associated period of oscillation, T_0, of the center droplet. In all following experiments, the intensity of light on the boundary droplets is equal to I_c to minimize the effects of increased diffusion of Br_2 and stray light.

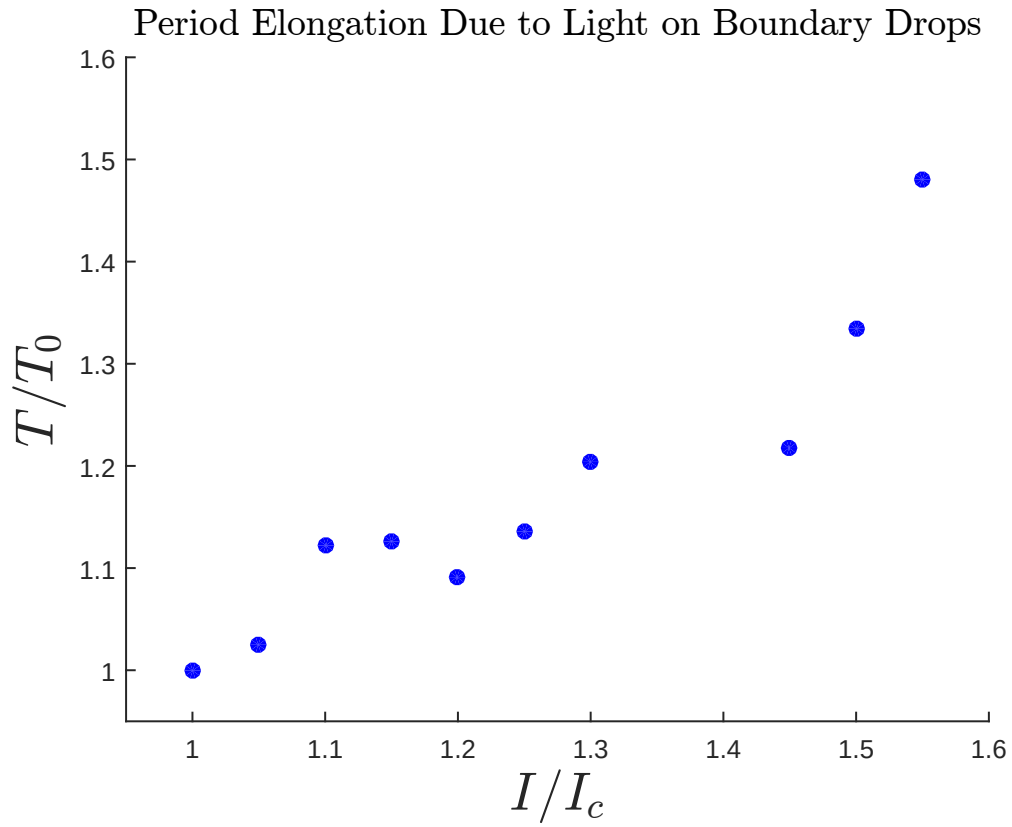

Figure 4.12: Plot of average period of the center droplet versus light intensity on boundary droplets, normalized by the critical intensity and associated period I_c and T_0.

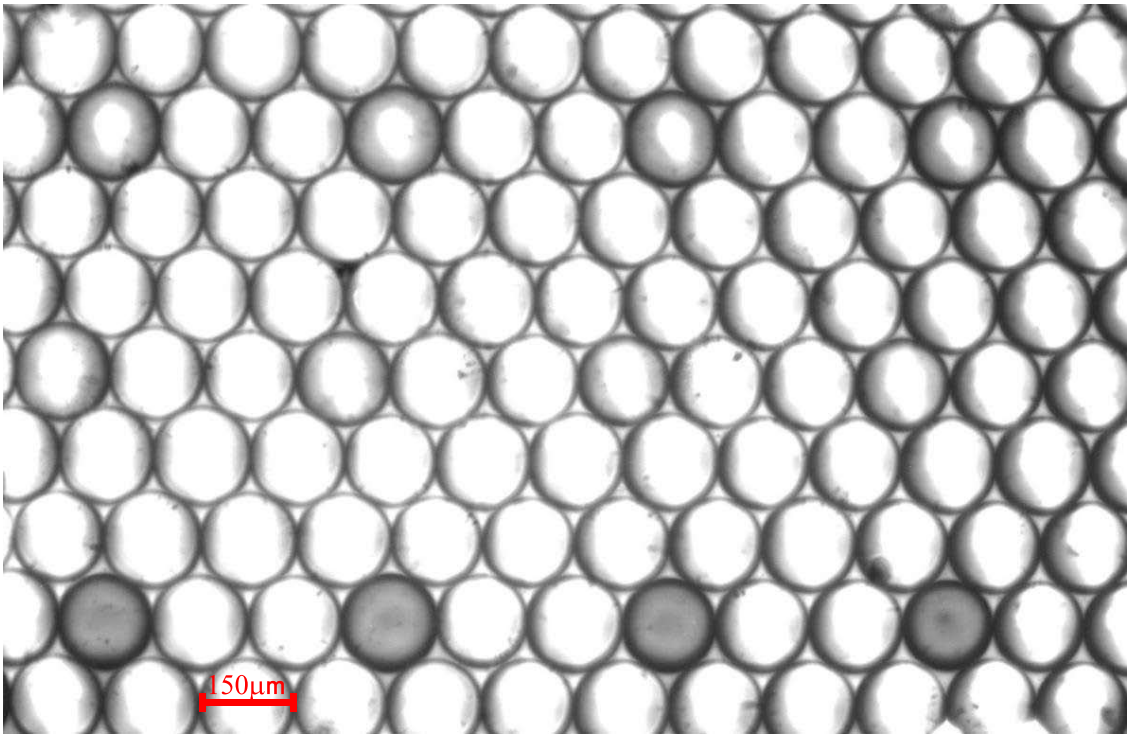

Figure 4.13: Image of an experiment varying the light intensity on optically isolated droplets with constant-chemical concentration boundaries to measure the period elongation curve (PEC) to light. Measurements are relative to the period of control droplets with no projected light (bottom row).

4.5 Period Elongation Curve

To quantitatively measure the effect of direct light on a droplet at intensities $I < I_c$, we created nearly identical optically isolated droplets with constant-chemical boundary conditions (see Figure 4.13). The isolated droplets were then constantly illuminated with (high frequency pulsed) light at various intensities. The droplets were divided into three categories:

(i) Control droplets with no projected light.

(ii) Droplets with constant projected light at intensities near I_c.

(iii) Droplets with constant projected light at intensities below I_c.

Figure 4.13 provides an image of the sample during the experiment. (i) Control droplets are in the bottom row, (ii) droplets with intensities near I_c are in the middle, and (iii) droplets with intensities below I_c are in the top row. The periods of all droplets were measured with reference to the average period of the control droplets and the results are plotted in Figure 4.14a. As the intensity of light increases, so does the period of oscillation; furthermore, the period increases at a faster rate as $I \to I_c^-$. At intensities $I > I_c$, the period is infinite—no oscillations occur. This behavior is reminiscent of an infinite-period bifurcation. Near such a bifurcation, the amplitude of oscillation remains unchanged but the period increases as $(\mu_c - \mu)^{-1/2}$ for some bifurcation parameter μ [16]. Modeling our data accordingly as

$$\frac{T(I)}{T_0} = \alpha \left(1 - \frac{I}{I_c}\right)^{-1/2} + \beta, \tag{4.1}$$

where $\alpha = 0.1993$ and $\beta = 0.7226$ are constants, yields the fit in Figure 4.14b. It is interesting to note that at relatively low intensities of light ($I/I_c \approx 0.4$), the period of oscillation is shortened. This suggests an optically-induced excitatory pathway, though further investigation is needed.

4.5.1 Pulsed Light

As mentioned in Chapter 3, Section 3.3, we cannot shine truly constant light, but rather pulsed light with a 30% duty cycle: on for 3 seconds and off for 7. However, this high frequency pulsing agrees very well qualitatively with truly constant light achieved in the VE model. Figure 4.15 shows a simulated PEC with truly constant light that also exhibits extreme sensitivity at the bifurcation (though we see no period shortening). Figure 4.16 provides further evidence that suggests high frequency pulsed light is equivalent to constant light but at weaker intensities; in fact, it suggests that the total number of photons in a small time interval is the relevant quantity. A simulated trajectory with constant excitation rate $k(I_0)$ yields the same period as an excitation rate $(10/3)k(I_0)$ with a 30% duty cycle: on for 3 seconds, then off for 7.

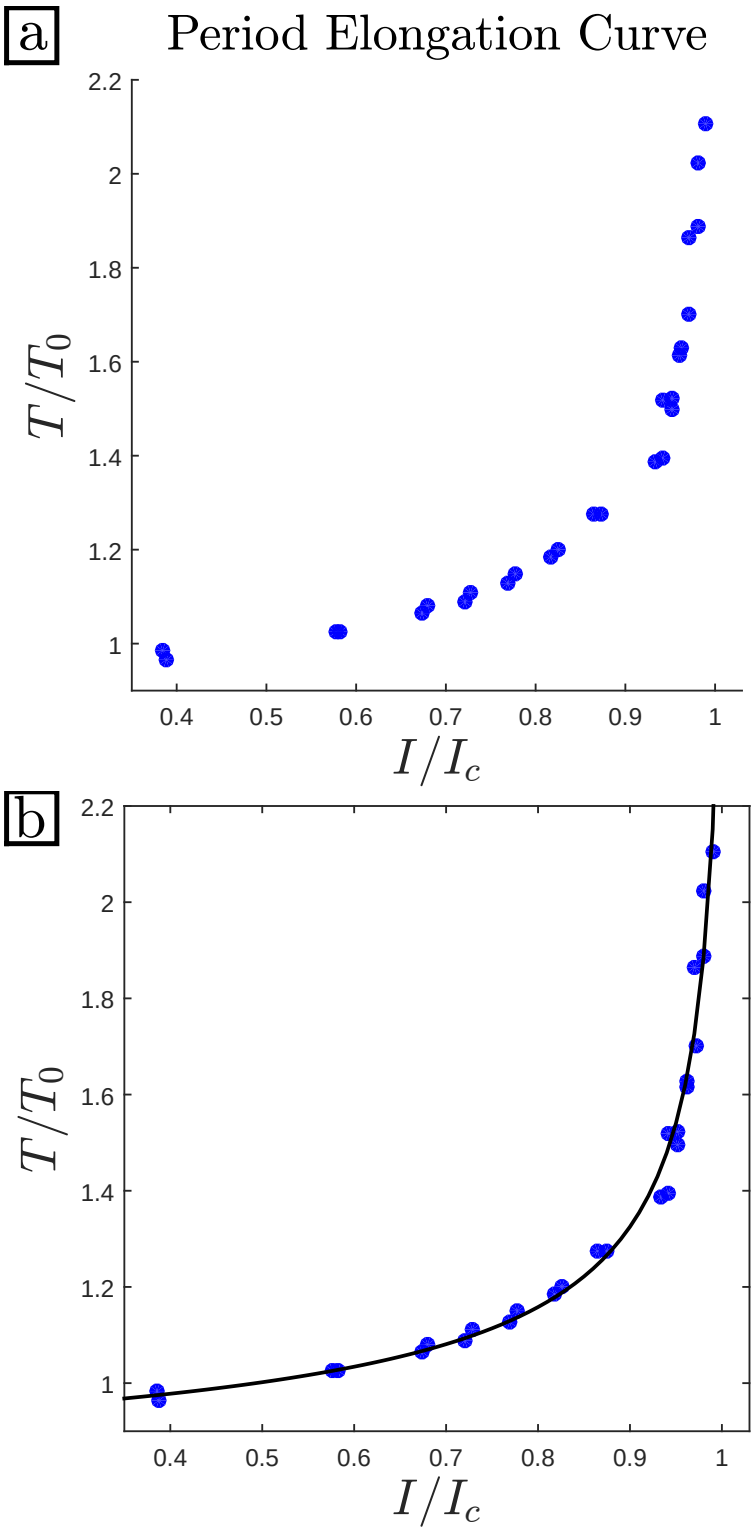

Figure 4.14: Period of optically isolated droplets with constant-chemical boundary conditions as a function of light intensity, normalized by the critical intensity I_c and period of control droplets T_0. (a) Raw data. (b) Fit using Equation (4.1).

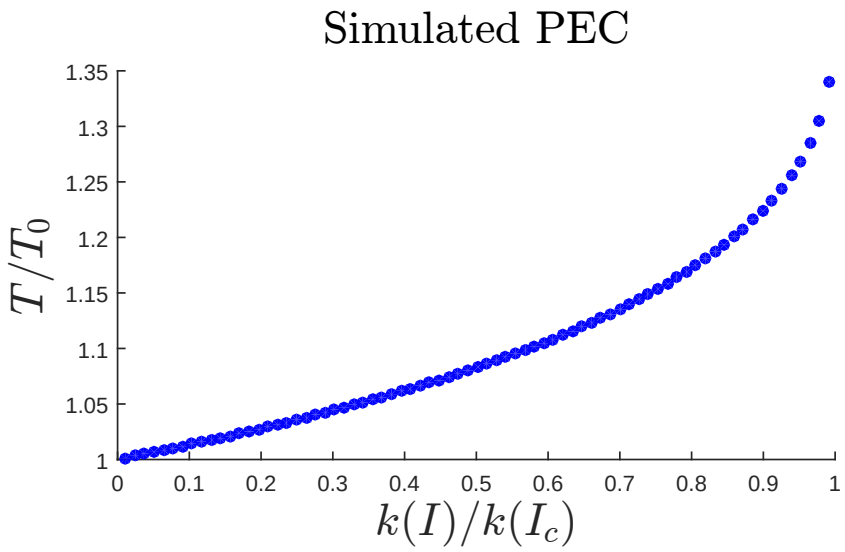

Figure 4.15: Simulated period elongation curve with truly constant light that exhibits similar qualitative behavior as measured in experiment with pulsed light (Figure 4.14).

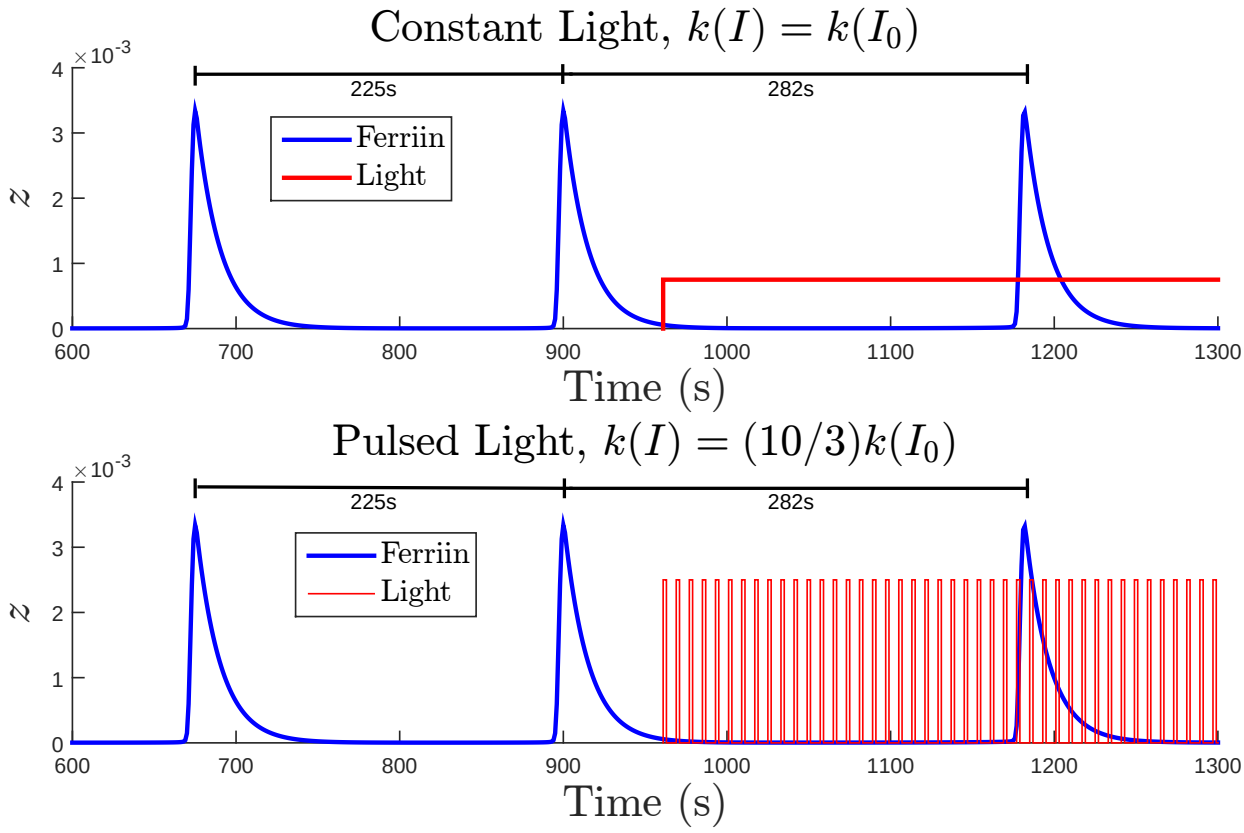

Figure 4.16: Simulated oscillations for constant light at $k(I) = k(I_0)$ (top) and pulsed light at a 30% duty cycle (3 s on, 7 s off) but at $k(I) = (10/3)k(I_0)$ (bottom). The elongation in period is exactly the same.

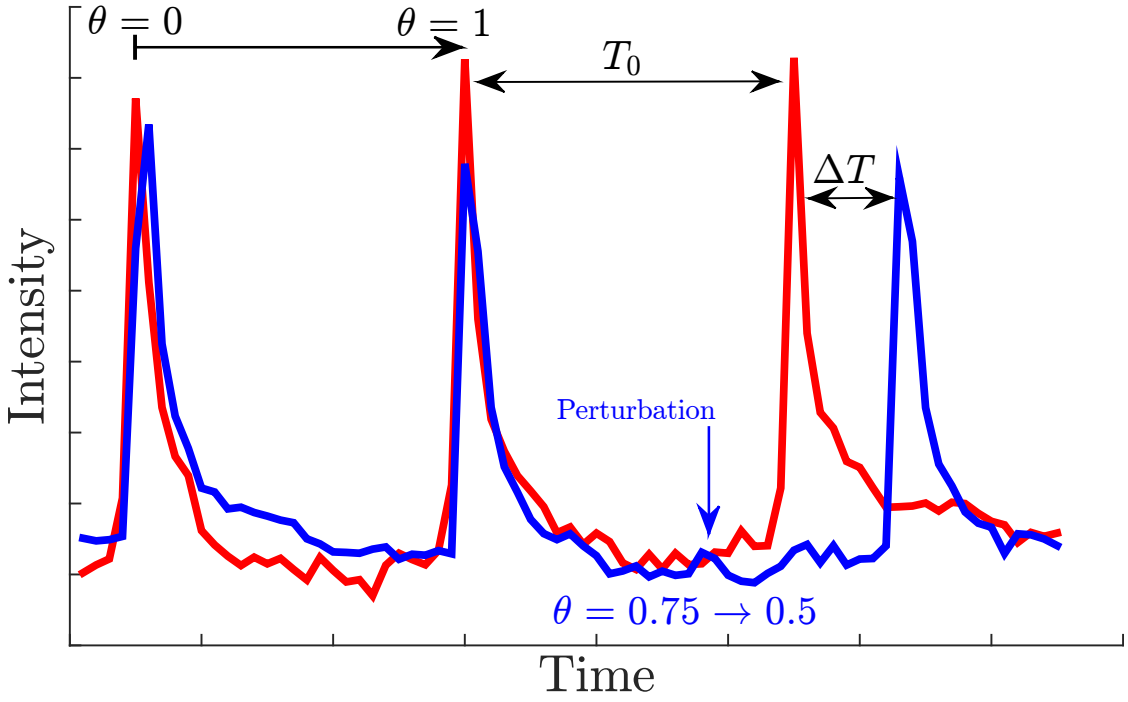

Figure 4.17: Intensity trace of an optically isolated droplet that is perturbed by a strong pulse of light. Peaks of intensity correspond to oxidation spikes. The initial oscillations are red and successive oscillations are blue, replotted to overlap the initial oscillations. This illustrates the period of oscillation is unchanged until the perturbation, delaying the last oxidation spike. The perturbation is timed near $\theta = 0.75$ to elicit the maximum response (See PRC in Figure 4.18) and delay the phase back to $\theta = 0.5$.

4.6 Phase Response Curve

Having established an inhibitory pathway via blue light, we investigated the effects of a strong, brief pulse of light rather than weaker, constant illumination discussed in Section 4.5. The optical perturbation tends to delay the oxidation spike of the next oscillation. Plotting the intensity of a perturbed droplet over time in Figure 4.17 illustrates this, where the time between peaks represents one period. The periods are identical until the perturbation, which delays the final oxidation spike considerably. Not all perturbations elicit such a large response, however.

To determine the effect of a perturbation in general, we construct a phase response curve

(PRC) from which we can deduce the transient change in the resultant oscillation. The PRC is a measure of how the phase of the oscillators changes when perturbed and is defined as

$$\mathrm{PRC}(\theta) \equiv \Delta\theta = 1 - \frac{T_0 + \Delta T}{T_0} \tag{4.2}$$

$$= -\frac{\Delta T}{T_0} \tag{4.3}$$

where θ is the phase of the perturbation, $\Delta\theta$ is the change in phase, T_0 is the unperturbed, natural period and ΔT is the change in cycle length containing the perturbation. Notice that if $\Delta T = 0$, that is to say the perturbation does not change the cycle length, then $\mathrm{PRC} = 0$. If $\Delta T > 0$, the extended cycle length due to the perturbation results in a phase delay since $\mathrm{PRC} < 0$. Similarly, if $\Delta T < 0$, then $\mathrm{PRC} > 0$ and there is a phase advance.

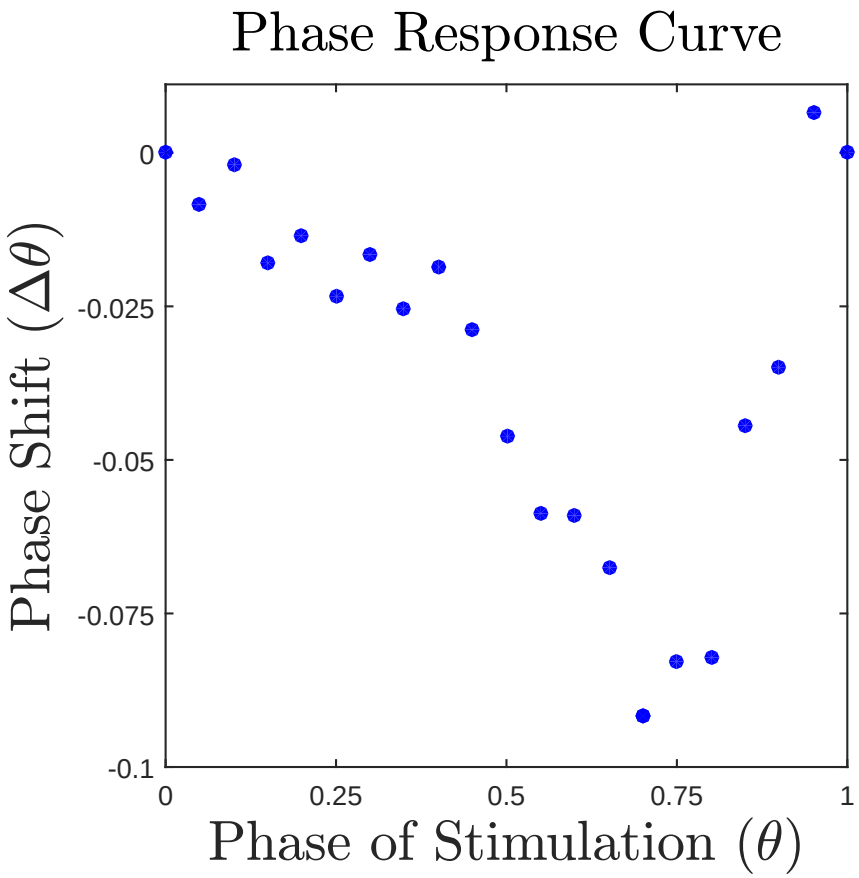

Figure 4.18: Experimental data for the optical PRC of an optically isolated droplet with constant-chemical concentration boundary conditions. It is mostly negative as expected due to inhibition via light, causing a phase delay. It is greatest in magnitude slightly before the next oxidation spike.

We measured the optical PRC of an optically isolated droplet experimentally by perturbing with light for $t_p < 0.01T_0$ at 20 different phases spaced evenly between 0 to 1 and measuring ΔT. The result is plotted in Figure 4.18. Simulating the chemical concentrations gives us insight to the shape of the PRC, specifically the concentration of inhibitor, y. A fitted curve to the PRC with associated chemical concentrations aligned at each phase is plotted in Figure 4.19. Notice that the decay rate of y is approximately exponential. Thus, if we treat a light perturbation as a constant addition of Δy to the oscillator, then a perturbation when $|dy/dt|$ is small and $dy/dt < 0$ will result in an increased length of time t until $y' = y + \Delta y$ returns to its original value of y. This is illustrated in Figure 4.20 where a perturbation is applied at two points, y_1 and y_2. The result is the same increase in concentration, Δy, yet a larger time $t_1 = 50$ s needed to return from $y_1' \rightarrow y_1$ as compared to $t_2 = 3$ s needed to return from $y_2' \rightarrow y_2$. Thus, a perturbation at y_1 will push the oscillator farther back in its limit cycle and cause a larger phase delay.

Treating a light perturbation in this way also explains the small regime of phase advance in the PRC. If the oscillator is perturbed when $dy/dt > 0$, then the oscillator will be pushed forward on the limit cycle. Notice, however, that there is a slight delay between the perturbation and the resultant increase in concentration. If the effect was immediate, then the PRC should be greatest in magnitude near $\theta = 1$, just before z peaks. The same qualitative behavior is present in a simulated optical PRC, shown in Figure 4.21. The data points just before $\theta = 1$ are slightly above zero.

In our experimentally measured PRC, the magnitude of the phase delay is less than 10%. This is the greatest delay we can achieve with a single three second light pulse in our system, but we can achieve larger delay with a sequence of pulses separated by 7 seconds in between each pulse (due to system limitations discussed in Chapter 3, Section 3.3). The three-pulse optical PRC is plotted in Figure 4.22 and allows us to achieve over 20% phase delay. We can further increase the phase delay by applying more pulses, or possibly increasing the concentration of photo-sensitive catalyst.

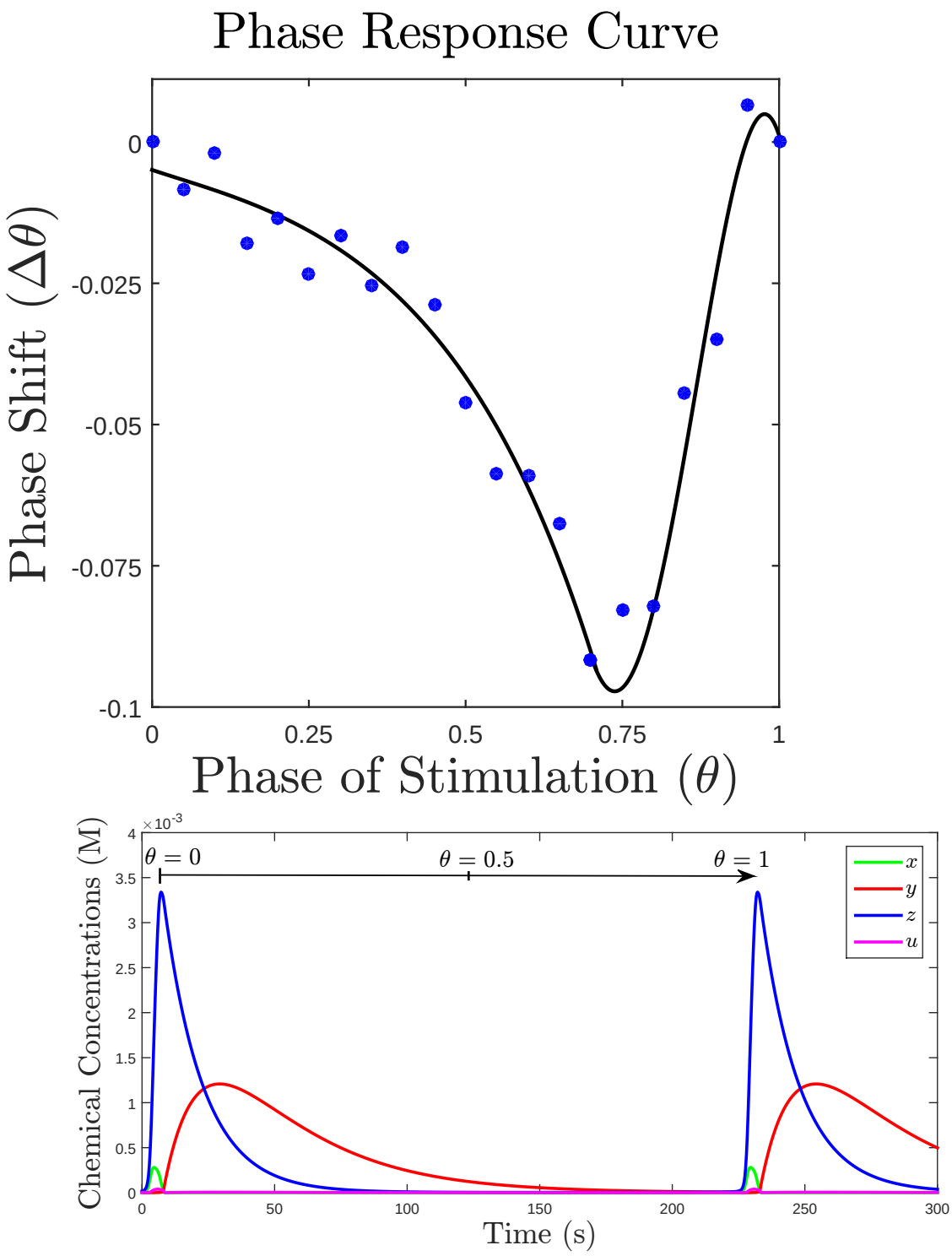

Figure 4.19: Optical PRC fit with simulated chemical concentrations aligned at each phase underneath.

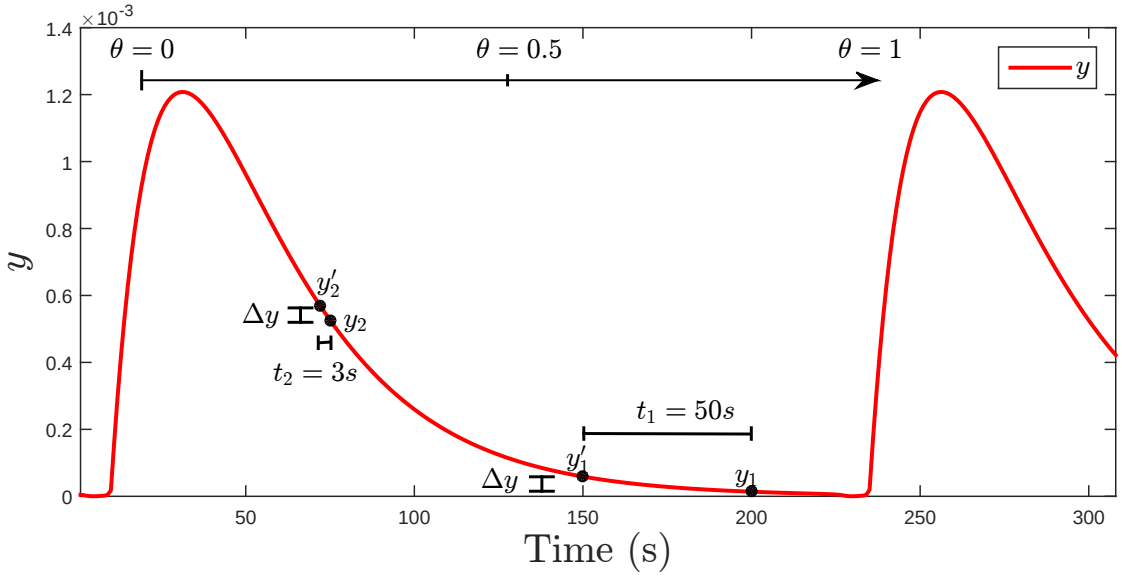

Figure 4.20: Concentrations of $y = [Br^-]$ illustrating different response times to a perturbation at two points, y_1 and y_2, corresponding to different phases. As a result, the phase response depends on the phase of stimulus.

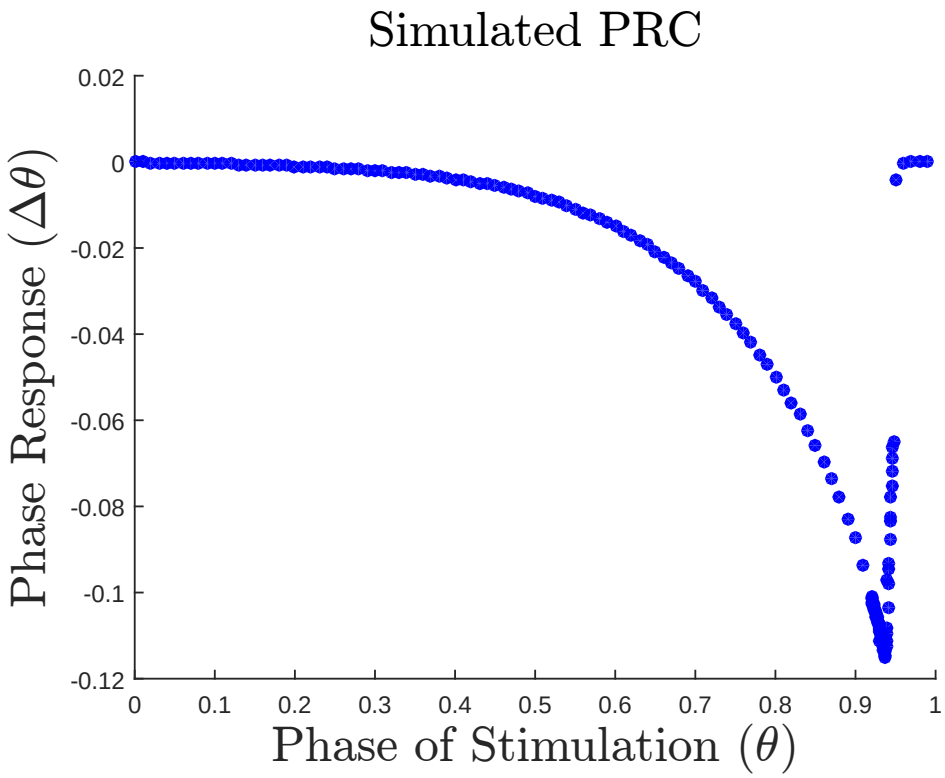

Figure 4.21: Simulated data for the optical PRC of an isolated droplet. As in the experimental PRC, it is greatest in magnitude before $\theta = 1$ and mostly negative, except for the few points just before $\theta = 1$.

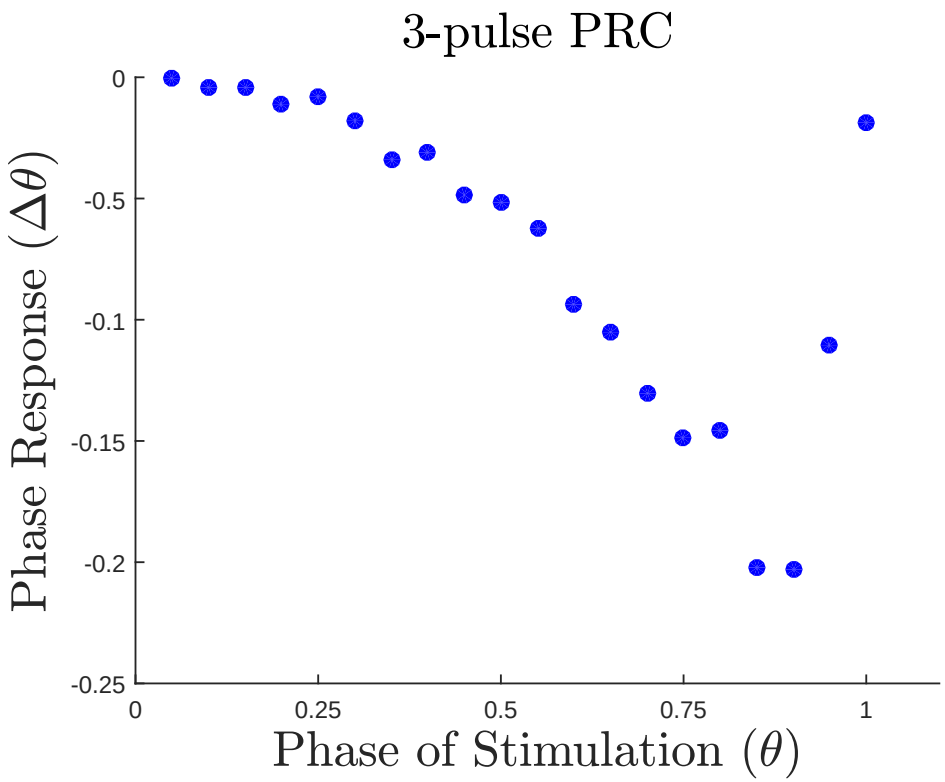

Figure 4.22: Experimental data for the three-pulse PRC, a sequence of three pulses separated by 7 s in between. This allows us to achieve a greater phase delay.

4.7 Future Work

In the experiments we have conducted measuring the PEC and PRC, we have only been able to achieve period elongation and phase delay. However, using the PEC and changing our definition of a perturbation, it is possible to achieve period shortening and hence phase advance. The PEC (Figure 4.14) suggests that constant, weak illumination can increase the period. In a sense, this allows us to shift the natural period of an oscillator by constantly projecting light. We can then give this elongated-period oscillator a "perturbation" by removing light temporarily. This will effectively decrease the concentration of inhibitor and hence advance the phase. The response of the oscillator, using the same formula (Equation 4.3), is what we call the dis-inhibition PRC, or dPRC. A simulation for the dPRC is shown in Figure 4.23 where light is removed for $t_p < 0.01T$. We can use the same reasoning as

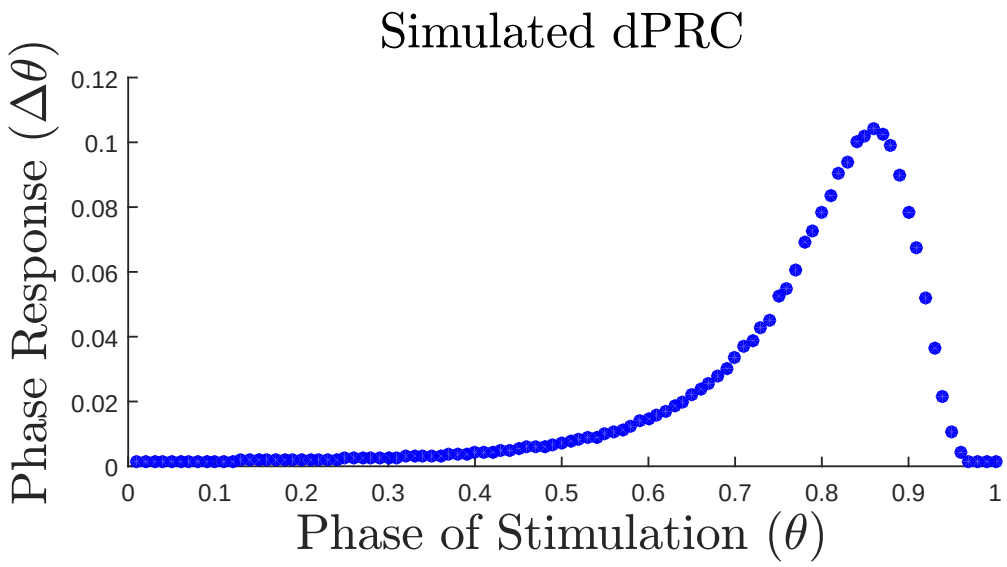

Figure 4.23: Phase response to a perturbation that briefly removes light on an otherwise constantly illuminated oscillator. The constant illumination increases the natural period, and hence removal of light causes a phase advance.

to why it is greatest in magnitude near $\theta \approx 0.9$; the effect of removing inhibitor is greatest when $|dy/dt|$ is small.

Now that we have characterized the effects of light on our system, we would like to use it to implement perturbations that shift the network from one attractor to another. The simplest non-trivial case consists of a triangular arrangement of oscillators that resembles a ring of three. It has been experimentally observed that there are two degenerate attractors: sequences of oscillations proceeding in a clockwise and counter-clockwise manner as indicated in Figure 4.24. Aside from the direction, they are mathematically equivalent with 3 phase clusters and a 1/3 phase separation between drops (as discussed in Section 4.1). One extreme method to switch between the two states is to suppress all oscillations and then selectively release light one at a time in the desired sequence. A more sophisticated method, supported in simulation, will not kill the oscillations entirely; rather, it consists of a perturbation on a single oscillator. Consider the traces in Figure 4.25 and notice the cyclic initial oscillations: red, green, blue, repeat. To switch the permutation, we suppress the red drop right before it would naturally spike but remove the light so that it spikes in between the expected green

and blue spike; this is enough to perturb the network into the second basin of attraction corresponding to the sequence: red, blue, green, repeat.

Moving forward, the next step would be to analyze larger networks, though the increasing complexity will require more sophisticated algorithms.

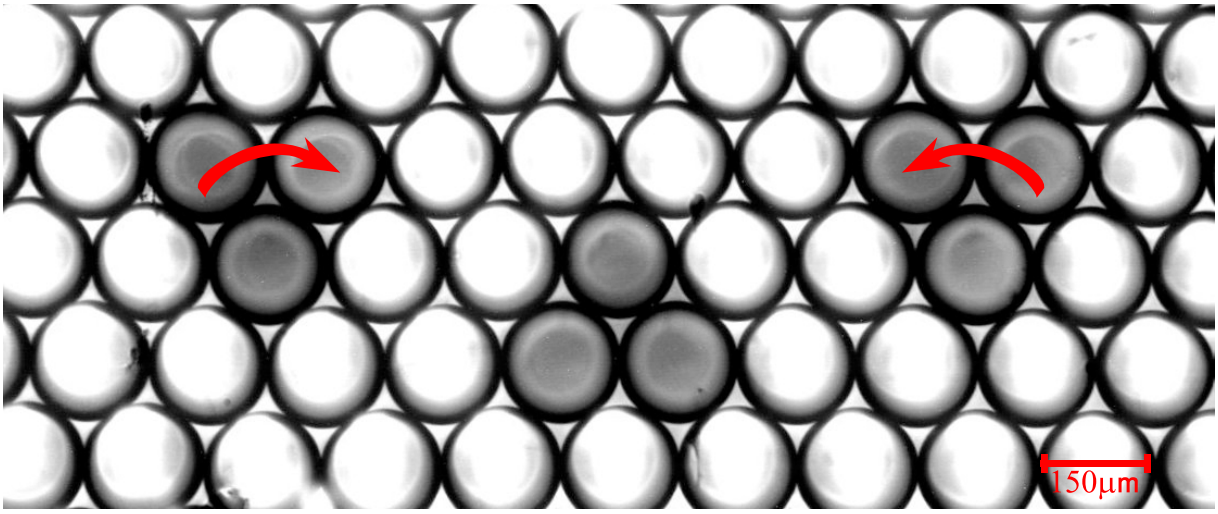

Figure 4.24: Optically isolated triangular rings of 3 oscillators in an emulsion. Two degenerate attractors are characterized by a clockwise and counter-clockwise sequence of oscillations.

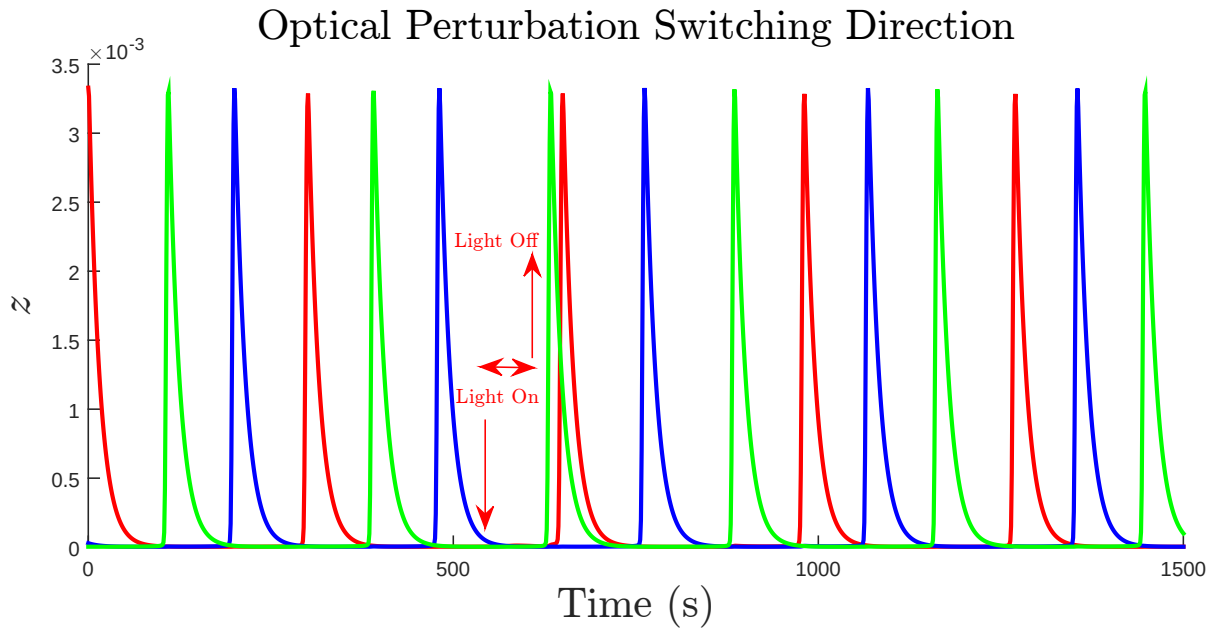

Figure 4.25: Simulated traces for a ring of three with initially cyclic oscillations in the sequence: red, green, blue. A perturbation on the red trace delaying its spike switches the sequence to red, blue, green.

Chapter 5

Chemical NOR Gate

There exist many forms of devices for computation including the familiar, like pocket calculators and personal computers, as well the unconventional, like elastic collisions of billiard balls [55], cellular automata [56], quantum computation [57], and neural networks [58, 59]. We are interested in chemical computation [60, 61, 62, 63] because it is fundamental to how living beings functions—through a series of chemical reactions.

Many implementations of chemical computation use reaction-diffusion systems, including the BZ reaction. Typically they are composed of large elements where spatial fluctuations propagate signals through excitatory waves, which are interpreted as Boolean values [63], though waves resulting in inhibition have been previously studied by our group [64]. The waves may collide and annihilate or propagate untouched, transmitting a signal. Other implementations are based on coupled continuously stirred tank reactors (CSTRs) utilizing bi-stable systems [60] and perturbations with activator and inhibitor injections [65]. CSTRs have been used to compute with fuzzy logic as well, which may be more comparable to computation in the brain [65]. However, these systems typically occupy milliliter volume.

We present a novel system using Boolean logic that is composed of nano-liter volume droplets containing the oscillatory BZ reaction coupled via inhibition.

Table 5.1: Truth table for a NOR gate.

Input 1	Input 2	NOR
0	**0**	**1**
0	**1**	**0**
1	**0**	**0**
1	**1**	**0**

5.1 Definition

A NOR gate is a two-input logic gate which outputs TRUE (T, logical 1) when both inputs are FALSE (F, logical 0), and outputs FALSE when one or both of the inputs are TRUE. Its truth table is shown in Table 5.1. To construct a NOR gate out of BZ droplets we need to leverage their dynamics in a way that satisfies this definition. The simplest choice for a TRUE input signal is an oxidation spike in a droplet indicated as the input to our gate, so a FALSE signal is a lack of oxidation spike (see Figure 5.2). For our gate to have the proper behavior, we must define the output in such a way that when one or both of our input droplets have an oxidation spike, the behavior of our output is distinguishable from the case when neither input spikes, but the difference between one and two spikes is indistinguishable.

Since any oxidation spike in one droplet results in diffusion of Br_2 that delays its neighbors' spikes (Chapter 4, Section 4.1), we can produce the desired behavior for our NOR gate consisting of three droplets: one central output between two inputs as shown in Figure 5.1. If either of the inputs spike, they will inhibit the oscillation of the output, causing it to spike later than expected. Since the output droplet will always eventually spike, we differentiate this from the case when neither input spikes through the use of a reading frame. We measure when the output is expected to spike based on its natural period and we also measure the delay we expect from one or two spikes. We choose a temporal window which ends after the output is expected to spike naturally but before it would spike if perturbed. By defining a spike before the window ends to be TRUE and after it ends to be FALSE, we can produce the behavior of a NOR gate as illustrated in Figure 5.2.

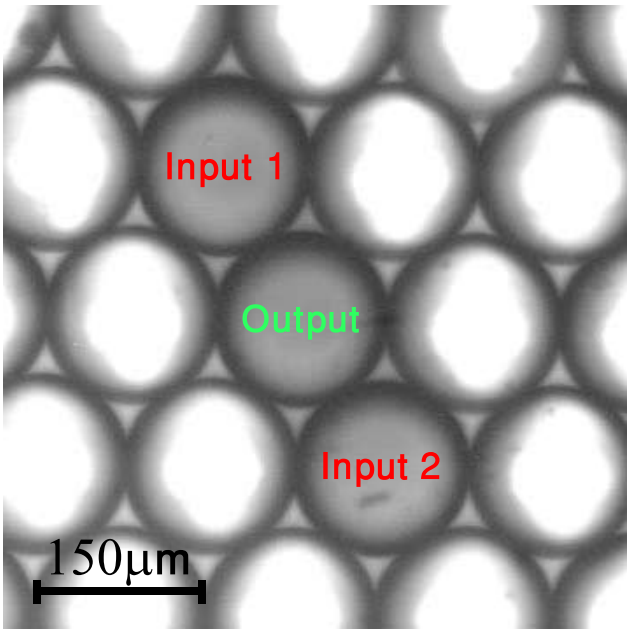

Figure 5.1: Definition of the inputs and output of our three-droplet NOR gate.

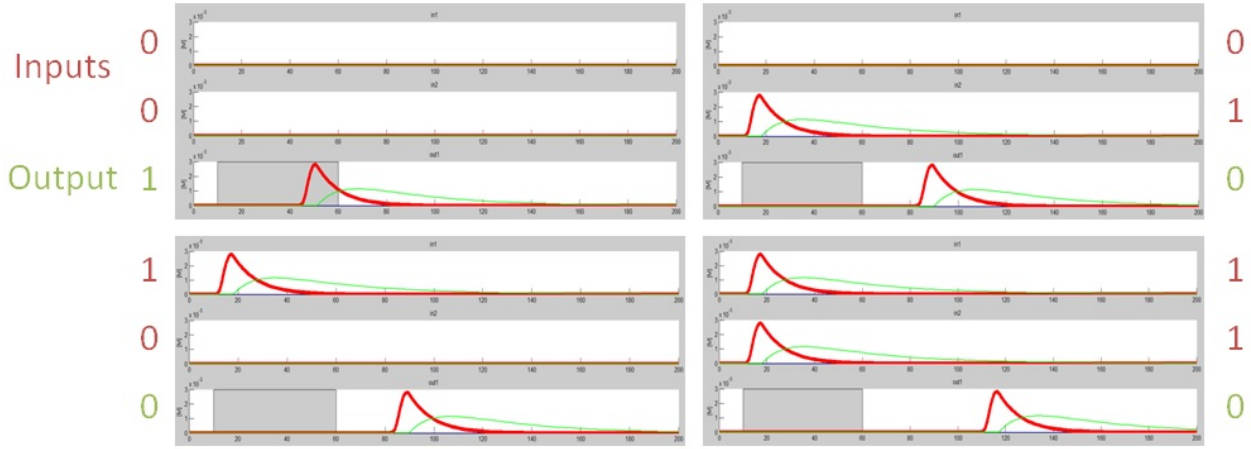

Figure 5.2: Simulated scenario illustrating a functional NOR gate where a TRUE input corresponds to the presence of an oxidation spike. When one or both of the inputs is true, the inhibitory coupling is enough to delay the spike of the output outside the chosen reading frame (gray rectangle), resulting in a FALSE output. Only when both inputs are FALSE results is no delay in the output such that it is captured within the reading frame, registering a TRUE output.

5.2 Characterization

There are several quantities we must measure to characterize our gate and verify that it functions reliably. First, the delay of the output's spike following a perturbation from an input must be significant enough that our reading frame correctly differentiates between TRUE and FALSE outputs. A larger delay means this can be accomplished more consistently. To maximize the delay resulting from a perturbation, we consult the one and two-droplet phase response curves. As in the optical PRC, this curve relates the change in phase of the output droplet as a function of the phase of the perturbation, where here the perturbations are oxidation spikes from one or two coupled droplets rather than light pulses. Having our inputs spike when they will produce the most negative phase shift, corresponding to the largest delay, will result in the optimal NOR gate behavior. The results for the one and two-droplet PRCs are plotted in Figure 5.3.

Second, we must be able to time the spike of the input such that it will induce a large delay in the output as governed by the PRCs. We suppress our input drops with light while they are not being used so if we want to send a FALSE input, they simply remain

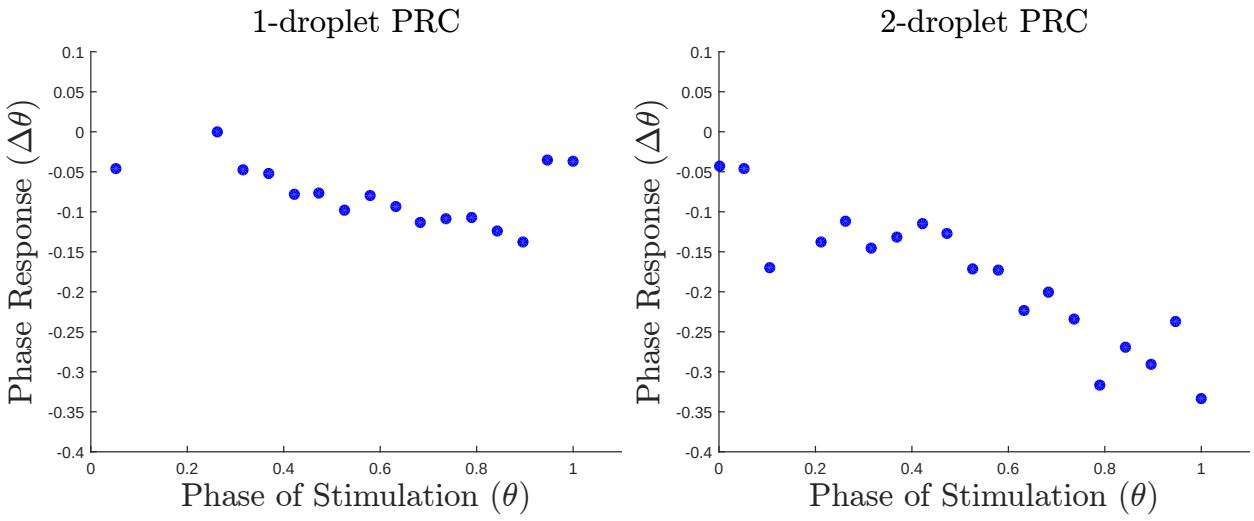

Figure 5.3: Phase response curve to perturbation by an oxidation spike from one and two coupled droplets. The spike results in diffusion of Br_2, which is converted to inhibitor and thus delays the phase.

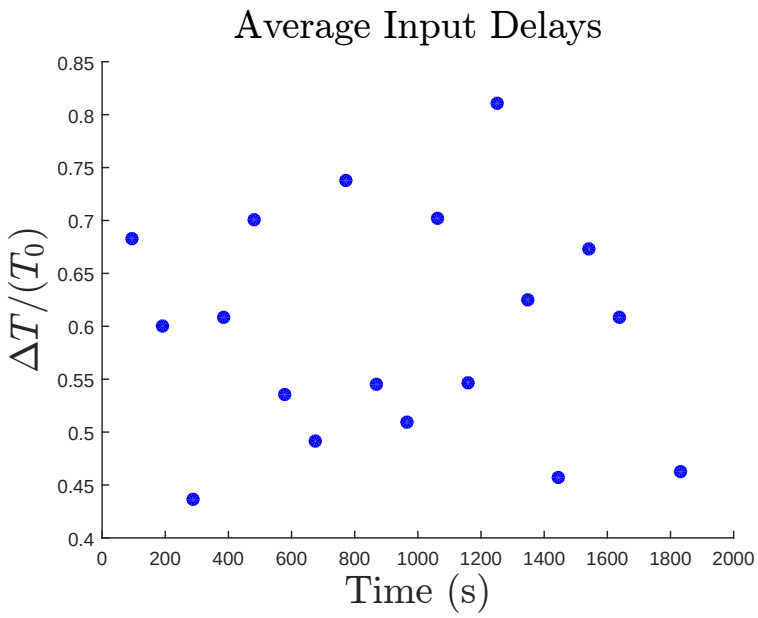

Figure 5.4: Plot of the average amount of time expected until an input spikes after light is removed, normalized by the natural period. The amount of time stays relatively constant throughout the experiment.

suppressed. If we want to send a TRUE input, we remove light until it spikes once, then resume illumination. Since we aim to have our inputs spike at a particular phase of the output droplet, we must measure the amount of time we expect to wait for them to spike once we remove light. The average spike delay is plotted in Figure 5.4.

5.3 Results

We determined the optimal phases to remove light from the inputs for all full NOR gate experiments by taking into consideration data from the one and two-droplet PRCs as well as the length of time it takes for a droplet to oscillate after removing light. We then cycled through the four input pairs and measured the response of the output. The results are plotted in Figure 5.5 with a representative reading frame where truth table 1 corresponds to the first set of 4 measurements, truth table 2 corresponds to the second set of 4 measurements, and so on. These results demonstrate that the T/F, F/T, and T/T input pairs indeed delay the

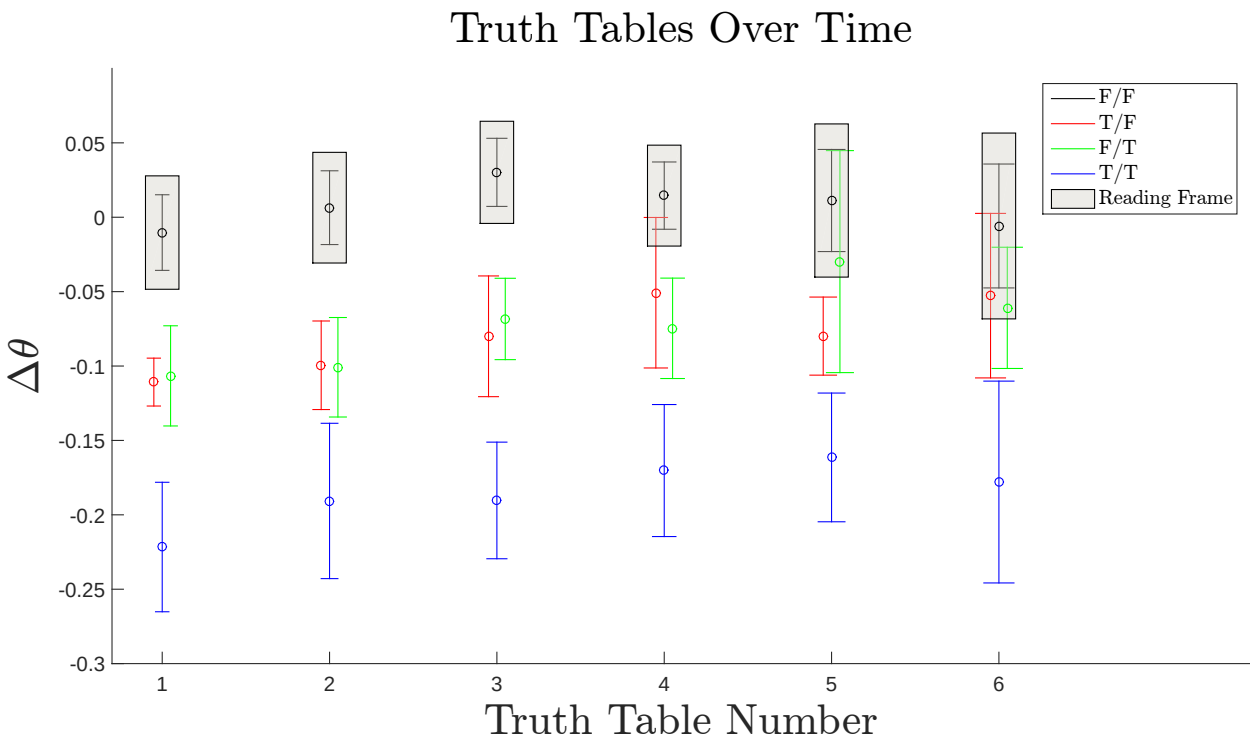

Figure 5.5: Output response to all four input pairs with a representative reading frame for each set of four measurements, constituting a NOR truth table. Increasing truth table number corresponds to increasing time of measurement. Due to chemical aging by light, later measurements yield higher variation in output response.

phase and hence delay the oxidation spike of the output a significant amount, while F/F induces no such delay—these are the necessary conditions for a functional NOR gate.

Notice, however, that the variation in response is much greater with increasing time. The first three truth tables yield fairly robust results, with all perturbations pushing the output spike outside the reading frame. The same cannot be said for tables 4 through 6, however. This can be attributed to chemical aging due to light since $Ru(bipy)_3$ is constantly oxidized in illuminated droplets. This increases the overall consumption of reactants, so prolonged suppression with light reduces the lifetime of the reaction and the oscillators no longer behave as we expect. This is confirmed in experiment where the inputs stop oscillating long before the output, which is never illuminated when measuring truth tables.

Another standard of the robustness of our NOR gate is the fraction of measured truth

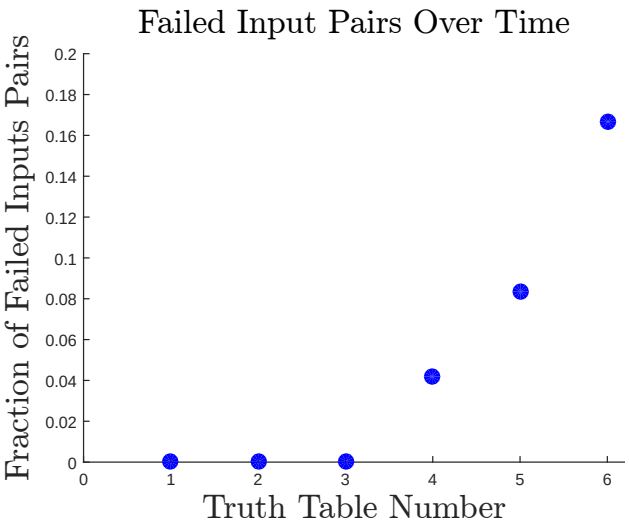

Figure 5.6: Fraction of failed input pairs over time.

tables that do not represent a NOR gate. We assume the F/F input pair to always yield TRUE by choosing our reading frame to contain the spike of F/F. Any case in which one or more of the other possible input pairs results in a spike that occurs before the F/F spike fails to compute NOR correctly. We consider the fraction of input pairs for which the output is incorrectly measured as TRUE as a standard of the performance of our gates. The fraction of inputs pairs that cause failed NOR gates is plotted in Figure 5.6. This again suggests that the number of failures increases over time, while the first few measured truth tables have a 100% success rate.

5.4 Future Work

There are multiple ways we envision improving the quality of our current gates. First, as a larger output delay from a TRUE input is more desirable, we plan to increase the delay by increasing the coupling strength between droplets. This can be achieved by reducing the size of our droplets or increasing the concentration of malonic acid [17]. Recall, for example, the 60 μm diameter droplets in Figure 3.4; it is in fact a pattern that is stationary in time due to the strong coupling strength [41].

Second, we can address the issue of our gates failing more over time by switching to an open system where we continuously flow new reactants in and old reactants out. Using a PDMS chip with wells to hold BZ, we can achieve a similar setup where the coupling strength is tuned by the well size and thickness of PDMS between wells; this controls the amount of Br_2 diffusing from well to well. This set-up also has the advantage that the gate configuration can be changed by simply altering the light projection; this may be useful if we are able to connect multiple gates and construct a circuit.

The main difficulty we will have to overcome to do so successfully is the fact that diffusion is naturally isotropic, so coupling an output droplet to the input droplet of another gate could cause that input to perturb the output, while an ideal circuit has outputs with infinite impedance. To get around this issue, we plan on externally entraining each droplet by flashing light on it twice per period. This would create two discrete states that each droplet would fall into: the state where it peaks after the first flash, or the state where it peaks after the second. Any significant perturbation would knock a droplet from one state into the other. This concept of light entrainment makes an open system critical in successfully connecting NOR gates to build larger circuits.

Chapter 6

Conclusions

We have successfully demonstrated the ability to engineer relevant geometries, including isolated droplets and rings, in a close-packed emulsion of micro-droplets containing the oscillatory Belousov—Zhabotinsky reaction. By adding a photo-sensitive catalyst, we have shown that we can optically perturb the oscillators to set initial conditions, elongate their natural periods, delay and advance their phase, and suppress their oscillations at will. These are crucial tools to engineer synchronization. Using these tools and a theoretical understanding of oscillators coupled via inhibition, we have shown in simulation that it is possible to perturb a ring of three oscillators between two attractors.

Moving forward, we will use technology we have manufactured to create custom planar networks of oscillators. The rings and star graphs in PDMS and silicon shown earlier in Figure 2.3 are representative examples of a few geometries we can engineer. The advantage of silicon, aside from being able to create custom geometries, is the different set of boundary conditions it imposes. Silicon is impermeable to flow, and hence provides no-flux boundary conditions. PDMS, on the other hand, will allow us to carefully tune coupling between droplets or wells, both in strength and type. The PDMS itself acts as a source of inhibitory coupling through diffusion of Br_2 and excitatory coupling can be created by connecting two wells together, hence allowing bulk BZ to flow from one well to another. Wells can also be

asymmetric, with one large node acting as a pace-maker connected to several smaller ones, for example. This may be useful in engineering a central pattern generator that can couple to a BZ gel and generate chemomechanical action.

We have also demonstrated a functional NOR gate composed of three BZ micro-droplets coupled via inhibition, which provides a basis for computation since the operation NOR is functionally complete. We have presented ideas to make the gate more robust by increasing coupling strength, improving controllability with light entrainment, and implementing an open system in PDMS. Since we are able to selectively suppress droplets in our experiments, these ideas establish the framework for connecting NOR gates together and building circuits for more sophisticated computations.

Bibliography

[1] Steven Strogatz. *SYNC: The Emerging Science of Spontaneous Order*. Hyperion, 2003.

[2] Steven H Strogatz, Ian Stewart, et al. "Coupled Oscillators and Biological Synchronization." *Scientific American*, **269**(6):102–109, 1993.

[3] Renato E Mirollo and Steven H Strogatz. "Synchronization of Pulse-Coupled Biological Oscillators." *SIAM Journal on Applied Mathematics*, **50**(6):1645–1662, 1990.

[4] John Jalife. "Mutual entrainment and electrical coupling as mechanisms for synchronous firing of rabbit sino-atrial pace-maker cells." *The Journal of Physiology*, **356**(1):221–243, 1984.

[5] Annette F Taylor, Mark R Tinsley, Fang Wang, Zhaoyang Huang, and Kenneth Showalter. "Dynamical Quorum Sensing and Synchronization in Large Populations of Chemical Oscillators." *Science*, **323**(5914):614–617, 2009.

[6] David J Schwab, Ania Baetica, and Pankaj Mehta. "Dynamical quorum-sensing in oscillators coupled through an external medium." *Physica D: Nonlinear Phenomena*, **241**(21):1782–1788, 2012.

[7] Bing-Wei Li, Chenbo Fu, Hong Zhang, and Xingang Wang. "Synchronization and quorum sensing in an ensemble of indirectly coupled chaotic oscillators." *Physical Review E*, **86**(4):046207, 2012.

[8] Eugene M Izhikevich. *Dynamical systems in neuroscience*. MIT press, 2007.

[9] Motoyasu Honma, Takatsune Kumada, Yoshihisa Osada, and Masayoshi Nagai. "Synchronized stepping: Automatic imitation behavior between persons." *The Japanese Journal of Psychonomic Science*, **27**(1):127–128, 2008.

[10] Michael J Richardson, Kerry L Marsh, Robert W Isenhower, Justin RL Goodman, and Richard C Schmidt. "Rocking together: Dynamics of intentional and unintentional interpersonal coordination." *Human Movement Science*, **26**(6):867–891, 2007.

[11] Wataru Sato and Sakiko Yoshikawa. "Spontaneous facial mimicry in response to dynamic facial expressions." *Cognition*, **104**(1):1–18, 2007.

[12] Irving R Epstein and John A Pojman. *An Introduction to Nonlinear Chemical Dynamics: Oscillations, Waves, Patterns, and Chaos*. Oxford University Press, USA, 1998.

[13] Arkady Pikovsky, Michael Rosenblum, Jurgen Kurths, and Robert C Hilborn. *Synchronization: A universal concept in nonlinear sciences*, volume 2. Cambridge University Press Cambridge, 2002.

[14] Yoshiki Kuramoto. *Chemical oscillations, waves, and turbulence*. Courier Corporation, 2003.

[15] Arthur T Winfree. *The geometry of biological time*, volume 12. Springer Science & Business Media, 2001.

[16] Steven H Strogatz. *Nonlinear Dynamics and Chaos: with Applications to Physics, Biology, Chemistry, and Engineering*. Westview Press, 2014.

[17] Vladimir K Vanag and Irving R Epstein. "Excitatory and inhibitory coupling in a one-dimensional array of Belousov–Zhabotinsky micro-oscillators: Theory." *Physical Review E*, **84**(6):066209, 2011.

[18] Charles S Peirce. "A Boolean algebra with one constant." *Collected papers of Charles Sanders Peirce*, **4**:1931–35, 1880.

[19] Farid Gharagozloo, Marc Margolis, Barbara Tempesta, Eric Strother, and Farzad Najam. "Robot-assisted lobectomy for early-stage lung cancer: report of 100 consecutive cases." *The Annals of Thoracic Surgery*, **88**(2):380–384, 2009.

[20] Yoshihiro Saitoh, Minoru Kondoh, and Yukio Komatsu. "Driverless car travelling guide system.", August 8 1989. US Patent 4,855,656.

[21] Filip Ilievski, Aaron D Mazzeo, Robert F Shepherd, Xin Chen, and George M Whitesides. "Soft Robotics for Chemists." *Angewandte Chemie*, **123**(8):1930–1935, 2011.

[22] Sangbae Kim, Cecilia Laschi, and Barry Trimmer. "Soft robotics: a bioinspired evolution in robotics." *Trends in Biotechnology*, **31**(5):287–294, 2013.

[23] Alin Albu-Schaffer, Oliver Eiberger, Markus Grebenstein, Sami Haddadin, Christian Ott, Thomas Wimbock, Sebastian Wolf, and Gerd Hirzinger. "Soft Robotics." *Robotics & Automation Magazine, IEEE*, **15**(3):20–30, 2008.

[24] Deepak Trivedi, Christopher D Rahn, William M Kier, and Ian D Walker. "Soft robotics: Biological inspiration, state of the art, and future research." *Applied Bionics and Biomechanics*, **5**(3):99–117, 2008.

[25] Atsushi Suzuki and Toyoichi Tanaka. "Phase transition in polymer gels induced by visible light." *Nature*, **346**:345–347, 1990.

[26] Mitsuhiro Shibayama and Toyoichi Tanaka. "Volume phase transition and related phenomena of polymer gels." In "Responsive gels: volume transitions I," pages 1–62. Springer, 1993.

[27] Ye Zhang, Ning Li, Jorge Delgado, Ning Zhou, Ryo Yoshida, Seth Fraden, Irving R Epstein, and Bing Xu. "Structural modulation of self-oscillating gels: changing the proximity of the catalyst to the polymer backbone to tailor chemomechanical oscillation." *Soft Matter*, **8**(26):7056–7061, 2012.

[28] Ryo Yoshida, Toshikazu Takahashi, Tomohiko Yamaguchi, and Hisao Ichijo. "Self-Oscillating Gel." *Journal of the American Chemical Society*, **118**(21):5134–5135, 1996.

[29] Alexander Pechenkin. "BP Belousov and his reaction." *Journal of Biosciences*, **34**(3):365–371, 2009.

[30] Hirokazu Fukuda, Hiroki Morimura, and Shoichi Kai. "Global synchronization in two-dimensional lattices of discrete Belousov–Zhabotinsky oscillators." *Physica D: Nonlinear Phenomena*, **205**(1):80–86, 2005.

[31] Francesc Sagués and Irving R Epstein. "Nonlinear chemical dynamics." *Dalton transactions*, (7):1201–1217, 2003.

[32] Arthur T Winfree. "The Prehistory of the Belousov–Zhabotinsky Oscillator." *Journal of Chemical Education*, **61**(8):661, 1984.

[33] Vladimir K Vanag and Irving R Epstein. "Pattern Formation in a Tunable Medium: The Belousov–Zhabotinsky Reaction in an Aerosol OTMmicroemulsion." *Physical Review Letters*, **87**(22):228301, 2001.

[34] László Györgyi, Tamás Turányi, and Richard J Field. "Mechanistic Details of the Oscillatory Belousov–Zhabotinskii Reaction." *Journal of Physical Chemistry*, **94**(18):7162–7170, 1990.

[35] Richard M Noyes, Richard Field, and Endre Körös. "Oscillations in Chemical Systems. I. Detailed Mechanism in a System Showing Temporal Oscillations." *Journal of the American Chemical Society*, **94**(4):1394–1395, 1972.

[36] Anatoly M Zhabotinsky. "Periodic Liquid Phase Reactions." In "Proc. Acad. Sci. USSR," volume 157, pages 392–395. 1964.

[37] Kuppuswamy Kalyanasundaram. "Photophysics, Photochemistry and Solar Energy Conversion with tris(bipyridyl)ruthenium(II) and its Analogues." *Coordination Chemistry Reviews*, **46**:159–244, 1982.

[38] Sándor Kádár, Takashi Amemiya, and Kenneth Showalter. "Reaction Mechanism for Light Sensitivity of the $Ru(bpy)_3^{2+}$-Catalyzed Belousov–Zhabotinsky Reaction." *The Journal of Physical Chemistry A*, **101**(44):8200–8206, 1997.

[39] Vladimir K Vanag and Irving R Epstein. "A model for jumping and bubble waves in the Belousov–Zhabotinsky-aerosol OT system." *The Journal of Chemical Physics*, **131**(10):104512, 2009.

[40] Richard J Field and Richard M Noyes. "Oscillations in chemical systems. IV. Limit cycle behavior in a model of a real chemical reaction." *The Journal of Chemical Physics*, **60**(5):1877–1884, 1974.

[41] Nathan Tompkins, Ning Li, Camille Girabawe, Michael Heymann, G Bard Ermentrout, Irving R Epstein, and Seth Fraden. "Testing Turing's theory of morphogenesis in chemical cells." *Proceedings of the National Academy of Sciences*, **111**(12):4397–4402, 2014.

[42] J-P Eckmann and David Ruelle. "Ergodic theory of chaos and strange attractors." *Reviews of modern physics*, **57**(3):617, 1985.

[43] Keisuke Ota, Toshiaki Omori, Shigeo Watanabe, Hiroyoshi Miyakawa, Masato Okada, and Toru Aonishi. "Measurement of infinitesimal phase response curves from noisy real neurons." *Physical Review E*, **84**(4):041902, 2011.

[44] Theoden I Netoff, Corey D Acker, Jonathan C Bettencourt, and John A White. "Beyond Two-Cell Networks: Experimental Measurement of Neuronal Responses to Multiple Synaptic Inputs." *Journal of Computational Neuroscience*, **18**(3):287–295, 2005.

[45] D Cumin and CP Unsworth. "Generalising the Kuramoto model for the study of neuronal synchronisation in the brain." *Physica D: Nonlinear Phenomena*, **226**(2):181–196, 2007.

[46] C. Holtze, A. C. Rowat, J. J. Agresti, J. B. Hutchison, F. E. Angile, C. H. J. Schmitz, S. Koster, H. Duan, K. J. Humphry, R. A. Scanga, J. S. Johnson, D. Pisignano, and D. A. Weitz. "Biocompatible surfactants for water-in-fluorocarbon emulsions." *Lab on a Chip*, **8**(10):1632–1639, 2008.

[47] Masahiro Toiya, Vladimir K Vanag, and Irving R Epstein. "Diffusively Coupled Chemical Oscillators in a Microfluidic Assembly." *Angewandte Chemie*, **120**(40):7867–7869, 2008.

[48] Jorge Delgado, Ning Li, Marcin Leda, Hector O González-Ochoa, Seth Fraden, and Irving R Epstein. "Coupled oscillations in a 1D emulsion of Belousov–Zhabotinsky droplets." *Soft Matter*, **7**(7):3155–3167, 2011.

[49] Shelley L Anna, Nathalie Bontoux, and Howard A Stone. "Formation of dispersions using "flow focusing" in microchannels." *Applied Physics Letters*, **82**(3):364–366, 2003.

[50] Nathan Tompkins and Seth Fraden. "A programmable illumination microscope from low-cost and reused components." 2015. Submitted to *American Journal of Physics*.

[51] Eve Marder and Dirk Bucher. "Central pattern generators and the control of rhythmic movements." *Current Biology*, **11**(23):R986–R996, 2001.

[52] Peter A Tass. *Phase Resetting in Medicine and Biology: Stochastic Modelling and Data Analysis*, volume 172. Springer Science & Business Media, 2007.

[53] David J Christini and Leon Glass. "Introduction: Mapping and control of complex cardiac arrhythmias." *Chaos: An Interdisciplinary Journal of Nonlinear Science*, **12**(3):732–739, 2002.

[54] István Z Kiss, Craig G Rusin, Hiroshi Kori, and John L Hudson. "Engineering Complex Dynamical Structures: Sequential Patterns and Desynchronization." *Science*, **316**(5833):1886–1889, 2007.

[55] Edward Fredkin and Tommaso Toffoli. *Conservative logic*. Springer, 2002.

[56] Stephen Wolfram. "Universality and complexity in cellular automata." *Physica D: Nonlinear Phenomena*, **10**(1):1–35, 1984.

[57] Michael A Nielsen and Isaac L Chuang. *Quantum computation and quantum information*. Cambridge university press, 2010.

[58] John J Hopfield. "Neural networks and physical systems with emergent collective computational abilities." *Proceedings of the National Academy of Sciences*, **79**(8):2554–2558, 1982.

[59] John J Hopfield. "Neurons with graded response have collective computational properties like those of two-state neurons." *Proceedings of the National Academy of Sciences*, **81**(10):3088–3092, 1984.

[60] D Lebender and FW Schneider. "Logical Gates Using a Nonlinear Chemical Reaction." *The Journal of Physical Chemistry*, **98**(31):7533–7537, 1994.

[61] Agota Tóth and Kenneth Showalter. "Logic gates in excitable media." *The Journal of Chemical Physics*, **103**(6):2058–2066, 1995.

[62] Allen Hjelmfelt, Edward D Weinberger, and John Ross. "Chemical implementation of neural networks and Turing machines." *Proceedings of the National Academy of Sciences*, **88**(24):10983–10987, 1991.

[63] Andrew Adamatzky, Julian Holley, Peter Dittrich, Jerzy Gorecki, Ben De Lacy Costello, Klaus-Peter Zauner, and Larry Bull. "On architectures of circuits implemented in simulated Belousov–Zhabotinsky droplets." *BioSystems*, **109**(1):72–77, 2012.

[64] Michael Heymann, Kyle Ira Harrington, Jordan B Pollack, and Seth Fraden. "En Route to Signal Inversion in Chemical Computing." In "ALIFE," pages 166–167. 2010.

[65] Pier Luigi Gentili, Viktor Horvath, Vladimir K Vanag, and Irving R Epstein. "Belousov–Zhabotinsky 'Chemical Neuron' as a Binary and Fuzzy Logic Processor." *IJUC*, **8**(2):177–192, 2012.

Acknowledgements

I would like to thank Professor Seth Fraden for all his support and guidance as an advisor and mentor. He has been instrumental in my growth as a researcher and I owe many of my accomplishments to him.

I would like to thank Jacob Gold, who I have been collaborating with in some form since day one at Brandeis; it started with a hurricane and is ending with a degree, a destination, and a friendship.

I would like to thank Kyle Harrington for giving me the opportunity to work on this project, and for all the advice and help he has given me along the way. I would also like to thank Nate Tompkins for all his hard work, which has been crucial to the success of my research, as well Camille Girabawe for helping me run my first experiments in the lab.

Many thanks to Professor Paul Miller for being on my committee and Professor Irving Epstein for his willingness to help. I am also thankful to Kevan Hashemi for giving me my first opportunity to do research at Brandeis and Professor Leszek Malkinski, my REU advisor.

Finally, I would like to thank those closest to me—my family. 爸爸, 妈妈，哥哥: Thank you for supporting me for longer than I can remember. I wouldn't be where I am today without you.

爱你的琳琳